1997 IEEE International Ultrasonics Symposium
Short Course

Image Formation in Diagnostic Ultrasound

J. Nelson Wright

Consultant, Medical Imaging and Signal Processing

2672 Bayshore Parkway, Suite 532
Mountain View, CA 94043

650/969-1271 **FAX 650/969-1275**
jnwright@parallaxgroup.com

What is an Image?

Imaging as a Transformation

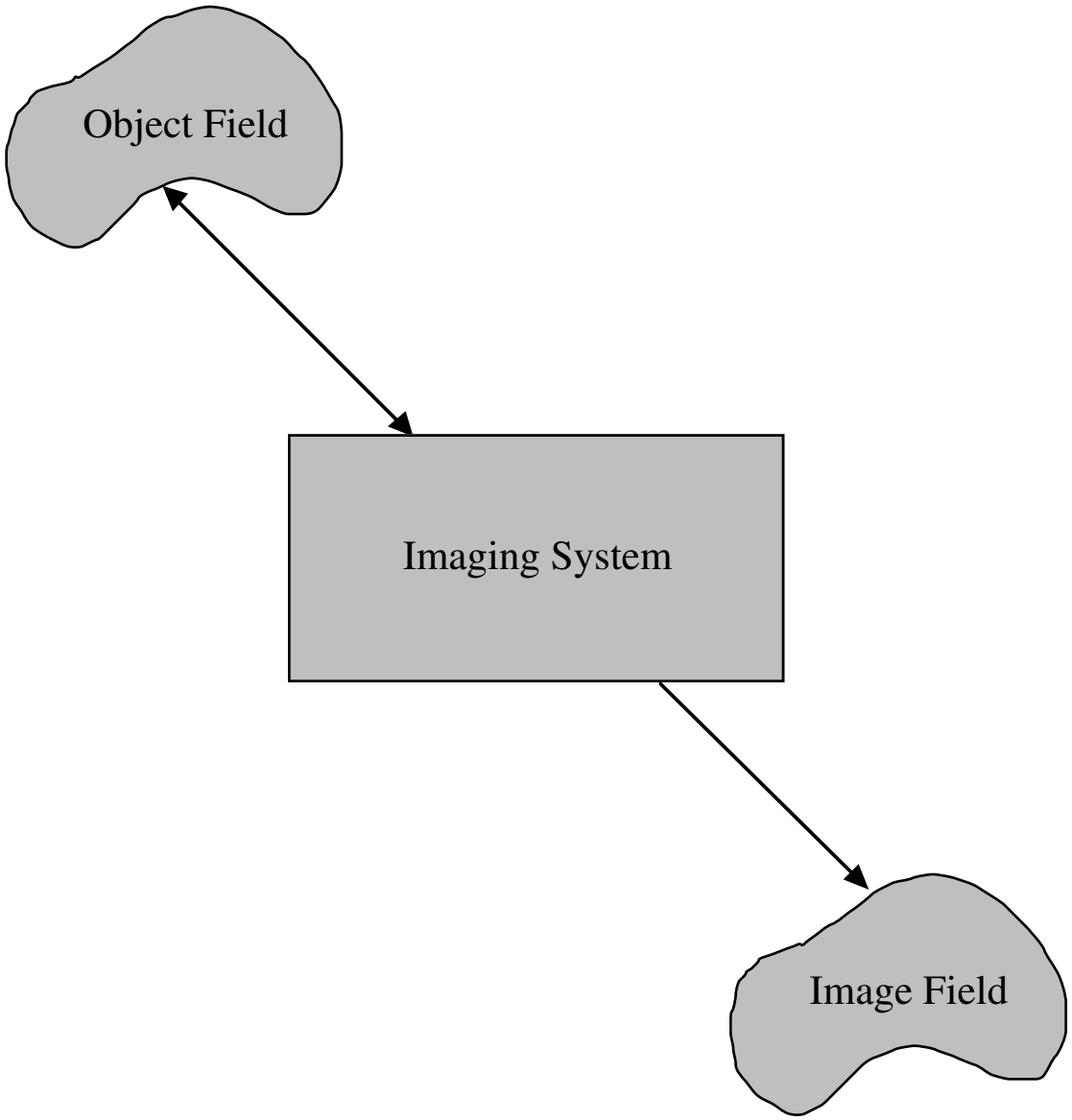

(1.1)

An image is a visual representation of a real object. An image is generally of *reduced dimensionality* and characterizes *some* of the object's properties.

An image is thus a *concrete abstraction* of the object.

Desirable Characteristics of an Imaging System

- Superposition
  The characteristic by which an image of two objects is the sum of two images of the individual objects, i.e., $I\{o_1 + o_2\} = I\{o_1\} + I\{o_2\}$.This is a local and global characteristic.

- Shift Invariance
  A characteristic by which small displacements between an object field and an imaging system result *only* in correspondingly small displacements of the resulting image field, i.e., if $I\{o(\mathbf{x})\} = i(\mathbf{x})$ then $I\{o(\mathbf{x}+\delta)\} = i(\mathbf{x}+\delta)$. This is a local characteristic.

- Image Uniformity
  The global characteristic by which desirable properties are maintained throughout the field of view.

Common Measures of Imaging System Performance

- Detail Resolution
  A measure of the minimum spacing of distinguishable point targets; this is a local characteristic.

- Contrast Resolution
  A measure of the differentiability of a region of one echogenecity within a region of different echogenecity. This is also a local characteristic.

- Temporal Resolution
  A measure of the number of independent images per unit time that can be acquired by an imaging system; this is a global characteristic.

- Dynamic Range
  The ability to simultaneously resolve small targets in the presence of large targets. This is both a local and global measure.

- Sensitivity
  The ability of the system to detect low level echoes. This is a global property.

Canonical Ultrasound Imaging System

All modern diagnostic ultrasound systems form their images using beamformers and arrays. While there are exceptions to this generalization, we won't investigate them in this course.

The block diagram of a canonical imaging system using beamformers is shown below.

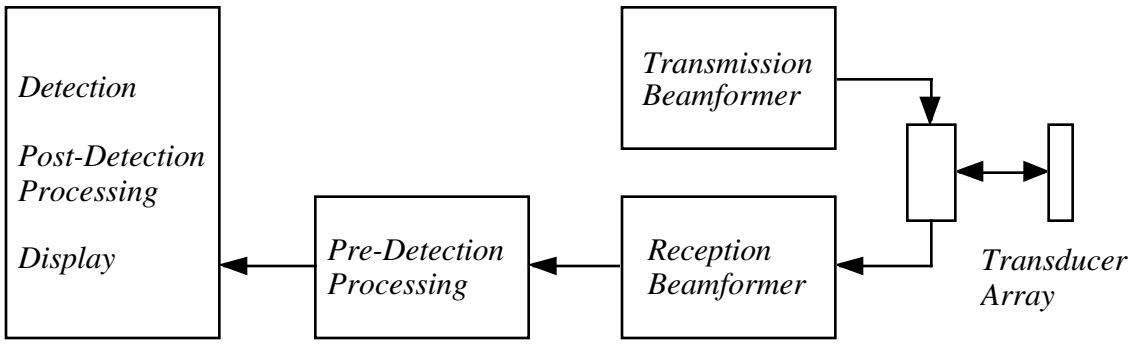

(1.2)

While we generally think of the image as that visual entity which appears on the screen, in this course we will take a somewhat narrower and more abstract view. We will focus our attention on beamformation and pre-detection processing, and we will usually think of the image as the abstract representation of the object field prior to detection. This abstract representation may or may not have a unified physical expression within any specific imaging system, but its characteristics are nonetheless central to the system's performance.

Linearity and shift-invariance are desirable characteristics of an imaging system. As we will see, acoustic propagation and diffraction are linear and shift-invariant, and we are naturally led to linear system theory to analyze, synthesize, and understand the process of image formation.

We start with the problem of focusing a linear acoustic aperture using geometrical optics, and deriving some basic geometrical relationships.

Apertures and Geometrical Optics

The Near Field/Far Field Crossover

Consider a uniform linear aperture of extent a excited with a monochromatic signal having wavelength λ. Consider a point target at a distance R from the aperture. The radiation from each incremental part of the aperture arrives at the target according to the propagation path length associated with the incremental aperture position and the target location. We can analyze this with the following figure.

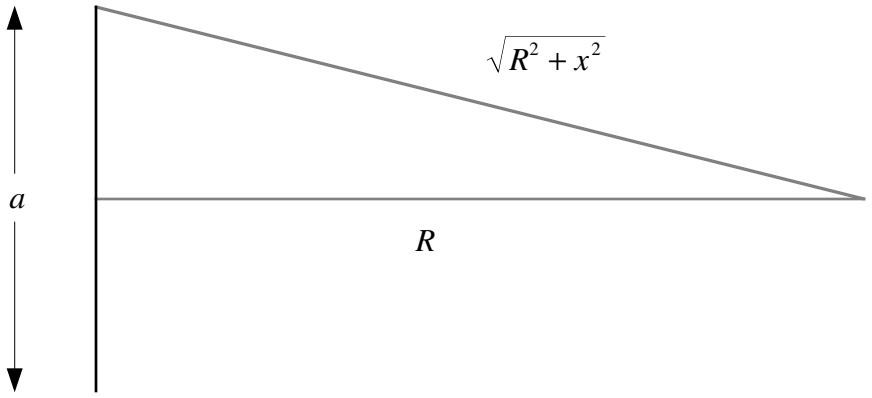

(2.1)

The differential path length Δ associated with a point x on the aperture and a range R can be evaluated using simple geometry.

$$\begin{aligned} \Delta &= \sqrt{R^2 + x^2} - R \\ &= R\sqrt{1 + \left(\frac{x}{R}\right)^2} - R \\ &\cong \frac{x^2}{2R} \end{aligned} \tag{2.2}$$

This differential error across the aperture is thus essentially quadratic, and can be reduced arbitrarily be increasing R. That is, in the far field the radiation from each point on the aperture arrives (essentially) coherently, adding constructively. As we move the point target closer to the aperture, the delay error increases inversely with R until, at some crossover range R_C between the near field and far field, it becomes non-negligible. We define this range $R = R_C$ (rather arbitrarily) as that for which the maximum error is

$$\Delta = \lambda/8 \tag{2.3}$$

As the maximum error will always be associated with the ends of the aperture, we substitute $x = a/2$ and use $\Delta = \lambda/8$ in eq. (2.2) to obtain

$$\boxed{\frac{R_C}{a} = \frac{a}{\lambda}} \tag{2.4}$$

That is, *the crossover range, measured in apertures, is equal to the aperture, measured in wavelengths.*

The far field is often called the *Fraunhofer region*, where we can ignore the differential phase terms associated with different propagation lengths. The near field is often called the *Fresnel region*, characterized by the (approximately) quadratic phase attributable to different propagation lengths from different aperture points.

Let us calculate the near field/far field crossover of a practical ultrasonic aperture operating at a center frequency of 3.5 MHz. Let

$$a = 28mm$$
$$\lambda = .44mm$$

This aperture might have 128 elements spaced at $\lambda/2$. The transition between the Fraunhofer region and the Fresnel region occurs at

$$R_C = 1782mm$$

or almost two meters! *All modern diagnostic ultrasonic imaging occurs in the extreme near field.* This distinguishes the discipline from many other imaging technologies and presents a notable engineering challenge.

We note that there are many alternative definitions of R_C possible, and they can be found in the literature. Outside of a specific engineering context, they are all rather arbitrary. Our choice is consistent with a delay error of one eighth of a wavelength, which may be devastating in some applications and benign in others. The designer of near field imaging systems has to be constantly aware of systematic phase errors (and their sources, and their effects) across the aperture.

Azimuthal Resolution and the Rayleigh Criterion of a Linear Aperture

Consider again a uniform linear aperture of extent *a* excited with a monochromatic signal having wavelength λ. Consider a point target in the far field, moved around a circular arc of constant range. Because we are in the far field, there is negligible phase error when the angle of the target is zero (i.e., the radiation from each aperture point arrives in phase). But as we traverse the circular arc, the phase error increases until some parts of the aperture start contributing destructively.

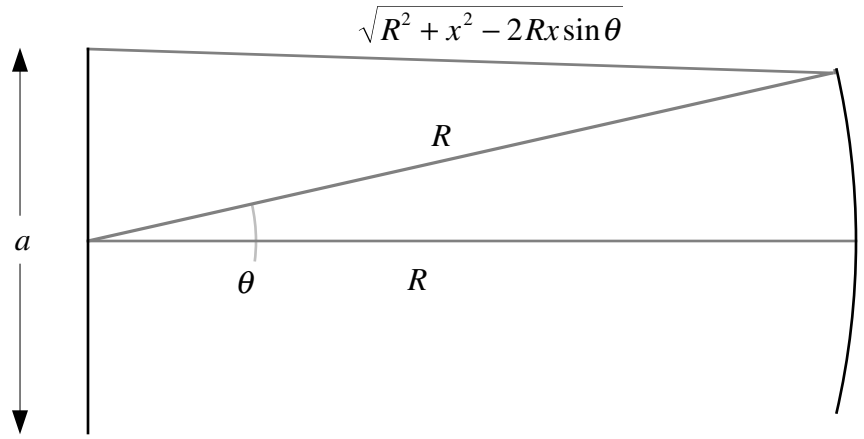

(2.5)

The differential path length Δ between an aperture point *x* and the center, as our point target moves along the circular arc, is

$$\begin{aligned}\Delta &= \sqrt{R^2 + x^2 - 2Rx\sin\theta} - R \\ &= R\sqrt{1 + \left(\frac{x}{R}\right)^2 - 2\left(\frac{x}{R}\right)\sin\theta} - R\end{aligned} \tag{2.6}$$

Expanding this in terms of x/R and θ

$$\begin{aligned}\Delta &\cong -x\theta + \frac{x^2}{2R} \\ &\cong -x\theta\end{aligned} \tag{2.7}$$

As in the last section, we ignore the quadratic term on the basis of far field operation.

Destructive interference occurs when the magnitude of any differential path length error exceeds $\lambda/4$, so we want to calculate the angular extent for which

$$-\lambda/4 \le \Delta \le \lambda/4 \tag{2.8}$$

As the maximum error will always be associated with the ends of the aperture, we substitute $x = \pm a/2$ and use $\Delta = \pm\lambda/4$ in eq. (2.7) to get the angles associated with this maximum error.

$$\theta|_{\Delta=\pm\lambda/4} = \pm\frac{\lambda}{2a} \tag{2.9}$$

We define this angular extent as the angular resolution θ_R.

$$\boxed{\theta_R = \frac{\lambda}{a}} \tag{2.10}$$

That is, *the angular resolution, measured in radians, is the inverse of the aperture, measured in wavelengths.*

It is also convenient to define the ratio of the range and the aperture, which re-occurs in different contexts, as the f-number.

$$\boxed{f_\# = \frac{R}{a}} \tag{2.11}$$

The distance around the circular arc associated with θ_R is simply $R\theta_R$, yielding the azimuthal resolution u_R.

$$\boxed{u_R = f_\#\lambda} \tag{2.12}$$

That is, *the azimuthal resolution, measured in wavelengths, is the f-number.*

Let us return to eq. (2.7) to consider the diffraction pattern as we traverse an arc in the far field. Let the arc length $u = R\theta$. A differential path length of $\Delta = -x\theta$ will induce a differential phase of $-2\pi\Delta/\lambda = 2\pi xu/R\lambda$ (the sign arising because a positive differential path length results in a later arrival time). If each incremental part of the aperture is radiating a complex exponential of the form $\exp(j2\pi f_0 t)$, then the ratio of the signal received at our point target to the total excitation signal is

$$\frac{\int_{-\frac{a}{2}}^{\frac{a}{2}} dx \exp\left(j2\pi\left[f_0 t - \Delta/\lambda\right]\right)}{\int_{-\frac{a}{2}}^{\frac{a}{2}} dx \exp\left(j2\pi f_0 t\right)} = \int_{-\frac{a}{2}}^{\frac{a}{2}} dx \exp\left(j2\pi\, xu/R\lambda\right)$$

$$= f_{\#}\lambda \int_{-\frac{1}{2f_{\#}\lambda}}^{\frac{1}{2f_{\#}\lambda}} dx \exp\left(j2\pi xu\right) \qquad (2.13)$$

$$= \operatorname{sinc}\left(\frac{u}{f_{\#}\lambda}\right)$$

This last integral is simply the (inverse) Fourier transform of $f_{\#}\lambda \operatorname{rect}\left(f_{\#}\lambda x\right)$, yielding the familiar sinc function for the far field diffraction pattern associated with a uniform linear aperture. Using eq. (2.13) to scale the abscissa, we see that $f_{\#}\lambda$ is the distance from the origin to the first zero; it is also a good measure of the width of the main lobe. It is commonly used as a measure of the resolving power of an optical system, and in that context is referred to as the Rayleigh criterion.

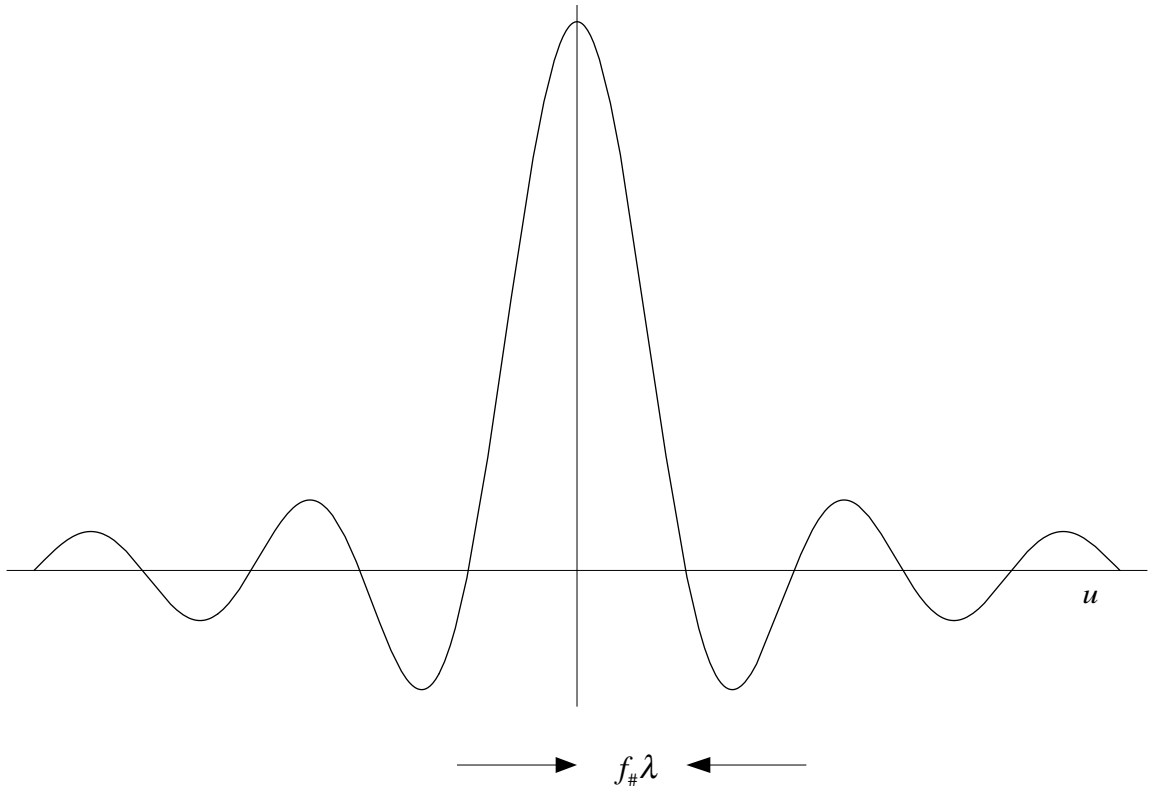

(2.14)

Let's consider an example. Suppose we have a reception aperture of $28mm$ operating at $\lambda = .220mm$, corresponding to 7 MHz. Immediately we see that our angular resolution in radians is $\theta_R = \lambda/a = 1/128$, corresponding to about $.45°$. If we have to scan through a $90°$ field of view with this aperture, we will need about 200 scan lines.

We hasten to add that this is a first-order approximation. In particular we have ignored the obliquity factor (the foreshortening of the aperture by the cosine of the steering angle) and the effects of two-way operation (the extra resolution afforded by the transmission beamformer). While these (and other) effects can be accommodated, geometrical optics is ultimately limited. Its principal virtue is its simplicity in concept and expression.

Depth of Focus of a Focused Linear Aperture

We can bring the far field diffraction pattern into the near field by *focusing* the aperture. This is done by applying compensating delays to incremental portions of the aperture. (In the figure below, we show the compensating delays as corrections to path length.)

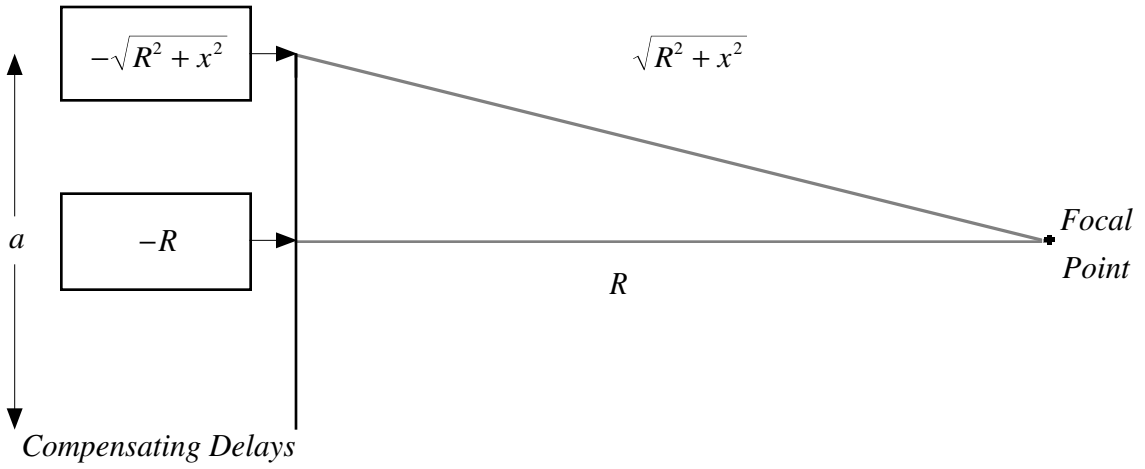

(2.15)

As we move a target along a circular arc through the focal point, we will measure the sinc function of fig. (2.14); this is because the compensating delays cancel, to first order, the differential delays associated with the near field. Our angular resolution is independent of our focal range R, but our azimuthal resolution improves as we focus further into the near field (because our f-number decreases with R). There is, of course, a price to pay for this improved resolution. As we move radially away from the focal point, the compensating delays no longer match the actual delays, and our azimuthal resolution degrades. We can estimate this depth of focus by considering the delay errors across the aperture as we move a point target a radial distance r from the focus.

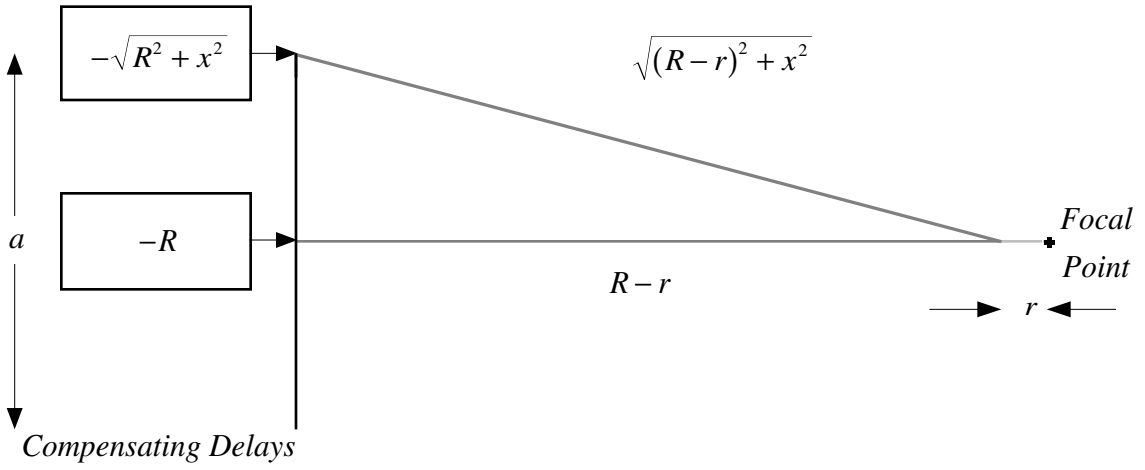

(2.16)

The differential delay between the center of the aperture and any other aperture point x (including the compensating delays) is

$$\begin{aligned}\Delta &= \left[\sqrt{(R-r)^2 + x^2} - \sqrt{R^2 + x^2}\right] - \left[(R-r) - R\right] \\ &= R\left[\sqrt{\left(1-\frac{r}{R}\right)^2 + \left(\frac{x}{R}\right)^2} - \sqrt{1+\left(\frac{x}{R}\right)^2} + \left(\frac{r}{R}\right)\right]\end{aligned} \tag{2.17}$$

Expanding this in a two dimensional Taylor's series in terms of r/R and x/R and keeping the lowest order term yields

$$\Delta = \frac{x^2 r}{2R^2} \tag{2.18}$$

The delay error across the aperture is thus seen to be essentially linear in *r* and quadratic in *x*. As we move closer to the aperture, the sign of the error is positive, and further away yields a negative error. Similar to our analysis of the near field/far field crossover, we define the depth of focus as the extent of the incremental range *r* for which

$$-\lambda/8 \le \Delta \le \lambda/8 \tag{2.19}$$

over the aperture. Substituting $x = a/2$ and $\Delta = \pm\lambda/8$ into eq. (2.18), and using $f_\# = R/a$, we see that the depth of focus is bounded by

$$r\big|_{\Delta=\pm\lambda/8} = \pm f_\#^2 \lambda \tag{2.20}$$

so the total depth of focus r_D is

$$\boxed{r_D = \pm f_\#^2 \lambda = 2 f_\#^2 \lambda} \tag{2.21}$$

That is, *the one-sided depth of focus, measured in wavelengths, is the square of the f-number.* Other definitions for r_D can be found in the literature, based on criteria other than the $\lambda/8$ differential error we have employed here. Let us look at the effects of moving our point target to the edge of the depth of focus and beyond.

Let our target traverse an arc of radius *R-r* in front of an aperture focused at *R*.

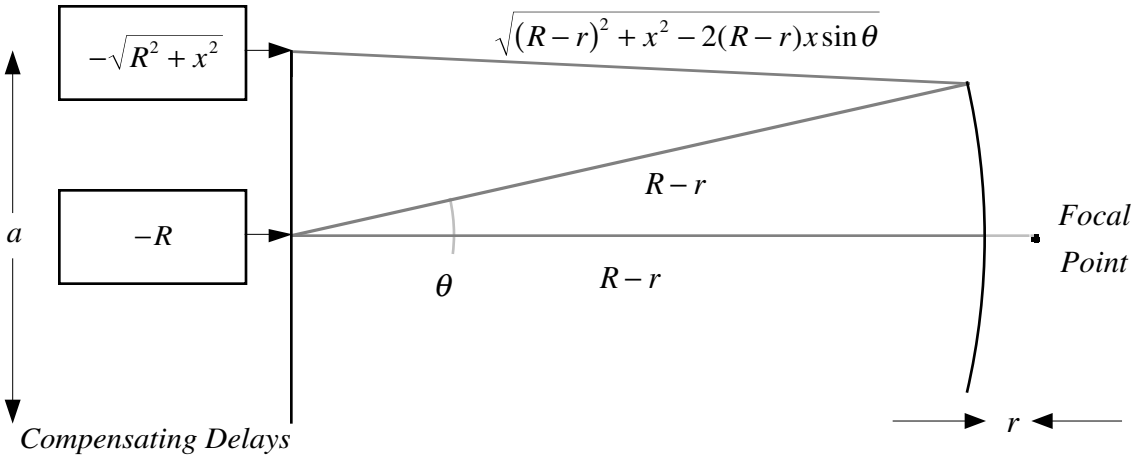

(2.22)

The differential delay is

$$\begin{aligned}\Delta &= \left[\sqrt{(R-r)^2+x^2-2(R-r)x\sin\theta}-\sqrt{R^2+x^2}\right]-\left[(R-r)-R\right]\\ &= R\left[\sqrt{\left(1-\frac{r}{R}\right)^2+\left(\frac{x}{R}\right)^2-2\left(1-\frac{r}{R}\right)\left(\frac{x}{R}\right)\sin\theta}-\sqrt{1+\left(\frac{x}{R}\right)^2}+\left(\frac{r}{R}\right)\right]\end{aligned} \tag{2.23}$$

Expanding this in a three dimensional Taylor's series in terms of r/R, x/R and θ, keeping the lowest order terms, and setting the arc length $u=\theta(R-r)$ yields

$$\begin{aligned}\Delta &\cong -\frac{xu}{R}\left[\frac{R+r}{R-r}\right]+\frac{x^2r}{2R^2}\\ &\cong -\frac{xu}{R}+\frac{x^2r}{2R^2}\end{aligned} \tag{2.24}$$

The diffraction pattern can be determined as in eq. (2.13).

$$\frac{1}{a}\int_{-\frac{a}{2}}^{\frac{a}{2}}dx\exp\left(j2\pi\left[xu/R\lambda-x^2r/2R^2\lambda\right]\right)=f_{\#}\lambda\int_{-\frac{1}{2f_{\#}\lambda}}^{\frac{1}{2f_{\#}\lambda}}dx\exp\left(-j2\pi x^2r\lambda/2\right)\exp\left(j2\pi xu\right) \tag{2.25}$$

This is the (inverse) Fourier transform of $f_{\#}\lambda\,\mathrm{rect}\left(f_{\#}\lambda x\right)\exp\left(-j2\pi x^2r\lambda/2\right)$, and of course when *r=0* it reduces to eq. (2.13). Below we plot the log magnitude of eq. (2.25) for different values of *r*.

Figure (2.26) is an idealized diffraction pattern of a focused linear aperture (i.e., a sinc function), plotted in decibels, when *r=0*.

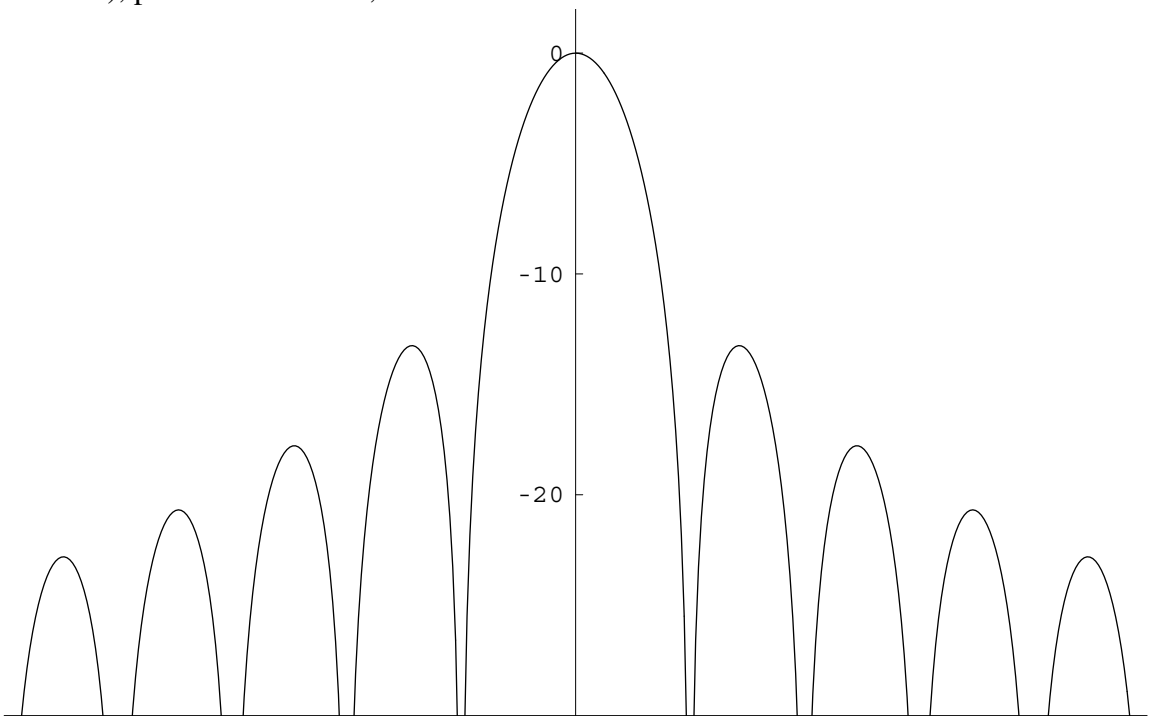

(2.26)

As the point target is moved to the edge of the depth of focus ($r = \pm f_{\#}^2 \lambda$) the diffraction pattern degrades due to the quadratic delay error peaking at $\pm\lambda/8$.

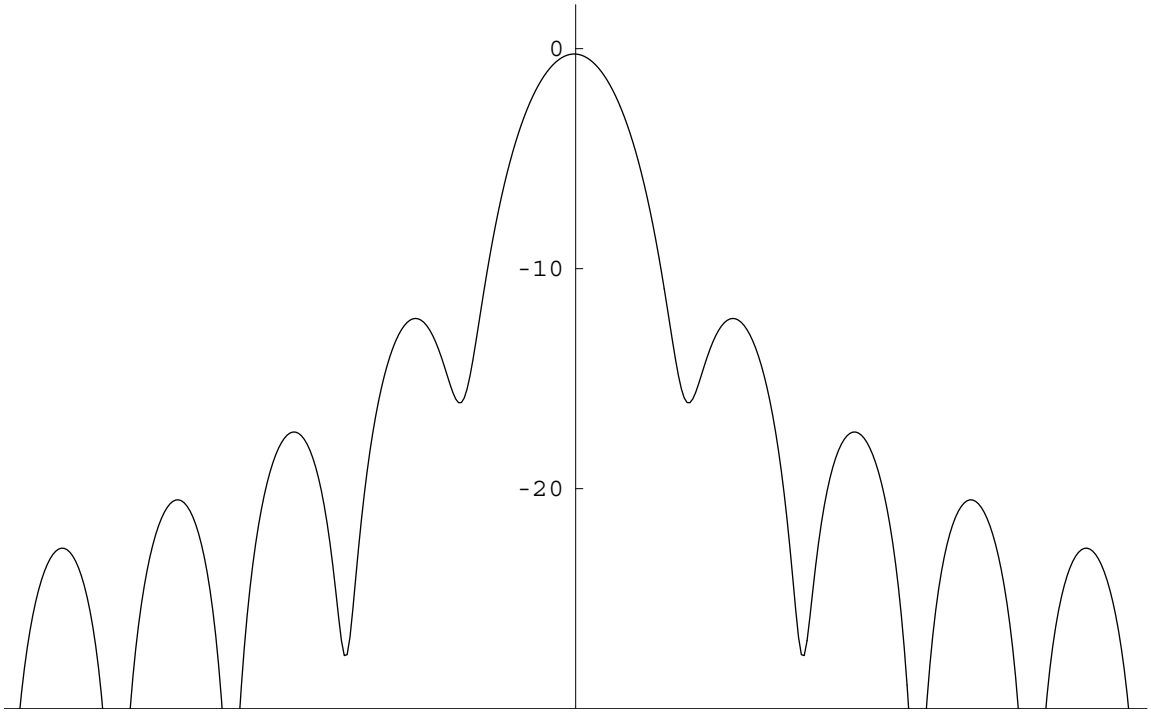

(2.27)

When we displace the target radially by $\pm 2 f_{\#}^2 \lambda$ (beyond the edge of the depth of focus), the quadratic delay error across our aperture peaks at $\pm \lambda / 4$.

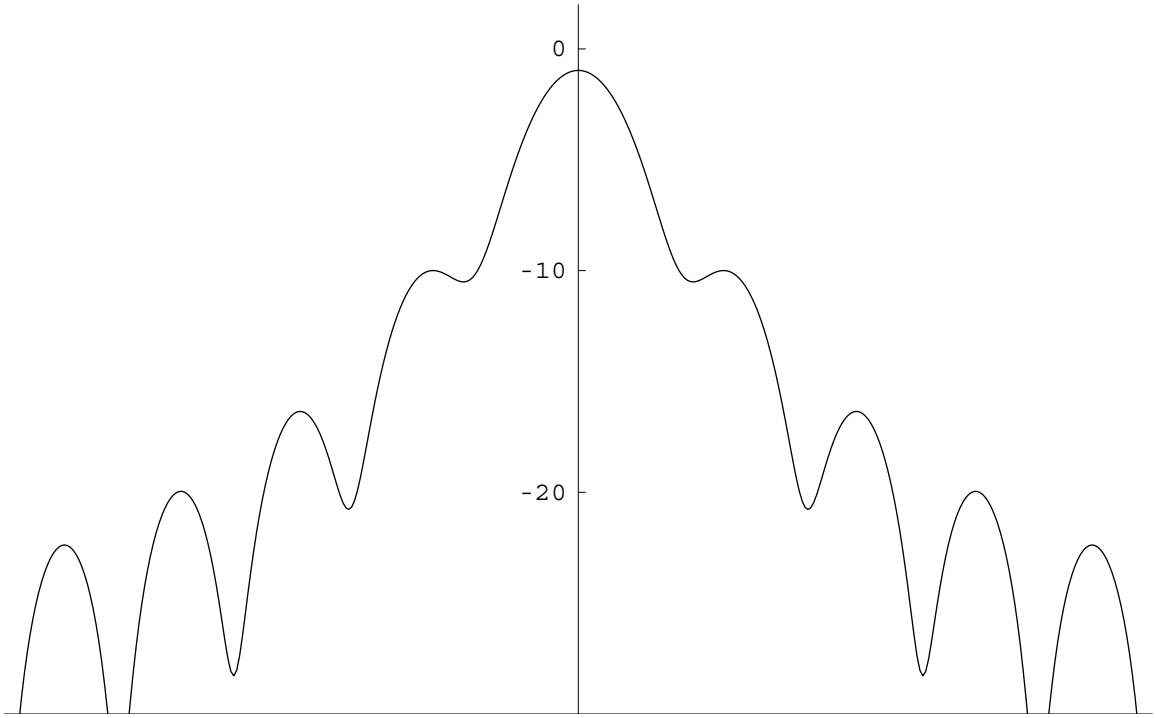

(2.28)

If we displace our target to $\pm 4 f_{\#}^2 \lambda$ (well out of the depth of focus) the diffraction pattern becomes severely distorted.

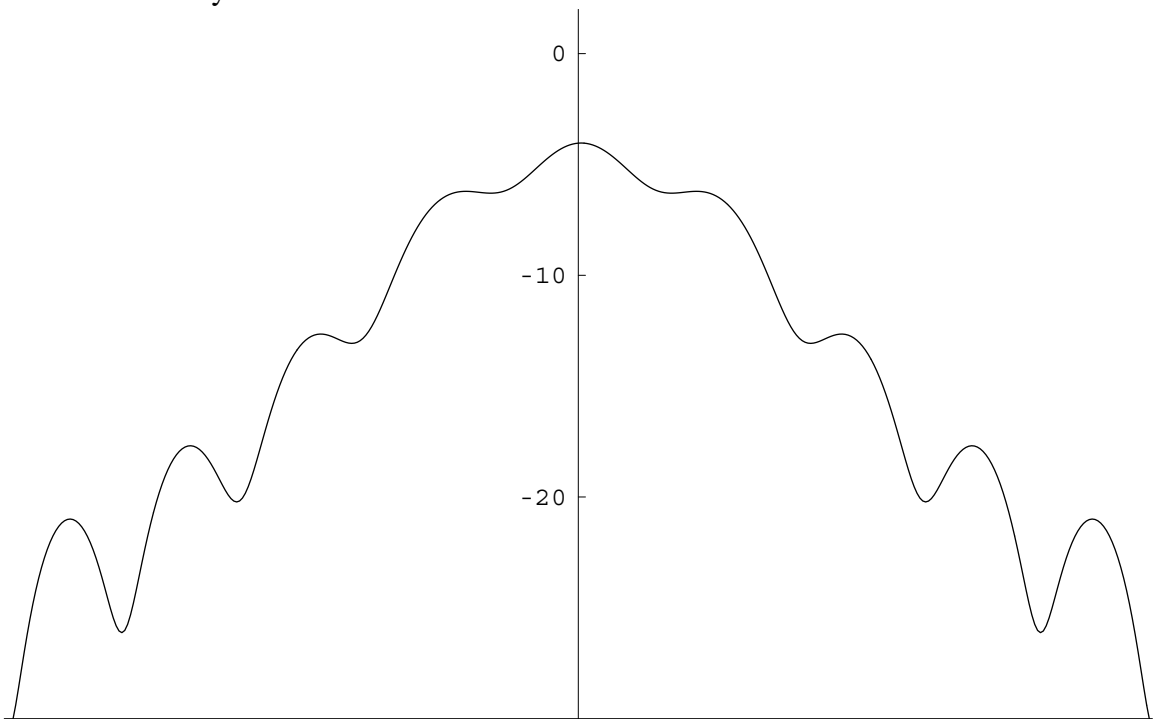

(2.29)

Depth of focus is a major engineering issue in the design of diagnostic ultrasound systems, because all modern systems use dynamic focusing on reception. This technology requires the compensating delays to be updated fast enough to focus on the echoes of a propagating pulse; each update has to be done in the round-trip propagation time of the depth of focus. Let's look at an example.

Consider a reception aperture working at $f_{\#} = 2$ and a center frequency of 5 MHz, corresponding to $\lambda = .308mm$. The depth of focus is thus $2.5mm$, and the round-trip propagation time (assuming the propagation velocity $c_0 = 1.54mm/\mu s$) is $3.2\mu s$. Thus every $3.2\mu s$ the aperture has to be re-focused in order to maintain the azimuthal resolution available with an f-number of two. If our reception beamformer has 128 channels, this requires that a new channel be updated, on average, every $25ns$.

More generally, if we are working with a center frequency of f_0, then a dynamic focused aperture has to be re-focused at a rate of $\left[2f_{\#}^2\lambda \cdot 2/c_0\right]^{-1} = f_0 \Big/ 4f_{\#}^2$.

The choice of $2f_{\#}^2/\lambda$ for our depth of focus is an historically conservative one, and ultimately has to be considered in a specific context. In ultrasound, the use of $4f_{\#}^2/\lambda$ and even $8f_{\#}^2/\lambda$ is not uncommon, and such liberties certainly ease the engineering difficulties associated with dynamic focusing. For modern high resolution imaging, however, these measures are inadequate.

Duality

Consider our aperture of extent *a* focused at range *R*, yielding azimuthal resolution $u_R = f_\# \lambda$. There is a dual of this system, which has an aperture of extent u_R focused at range *R* yielding azimuthal resolution *a*, as can be readily verified. In fact, this duality extends to other measures, as can be seen in the table below. Perhaps most interesting (and helpful to the memory) is that the depth of focus of our canonical system corresponds to the near field/far field crossover of our dual system.

Duality at Range *R*	System	Dual
Aperture	a	u_R
Azimuthal Resolution	u_R	a
f-number	$f_\#$	θ_R^{-1}
Angular Resolution	θ_R	$f_\#^{-1}$
Depth of Focus	$\pm f_\#^2 \lambda$	$\pm a^2/\lambda$
Near Field/Far Field Crossover	a^2/λ	$f_\#^2 \lambda$

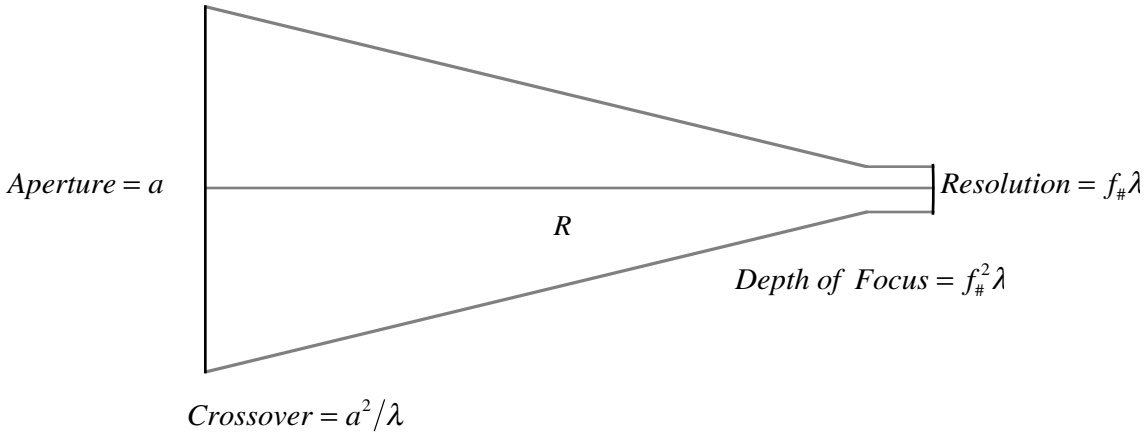

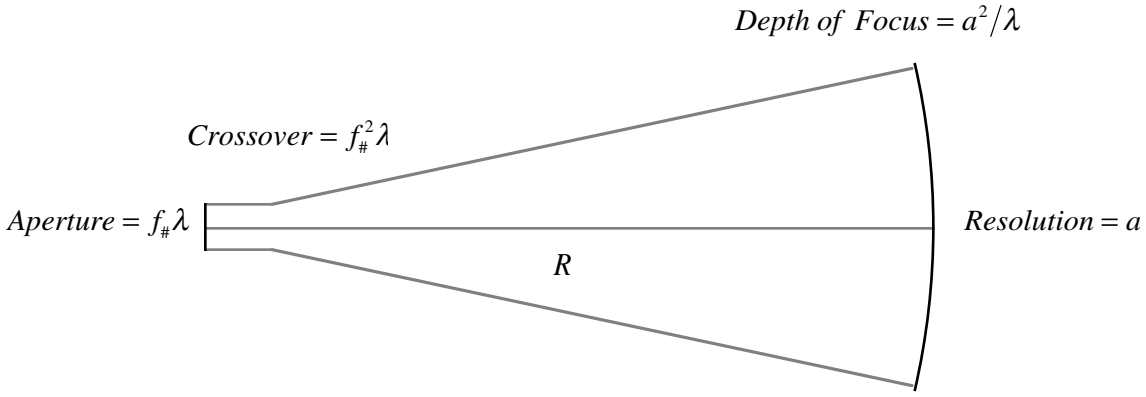

(2.30)

There is one range that has a special significance in this scheme: when we set $R = R_C$ (the near field/far field crossover) then *our system becomes the dual of itself*.

Duality at Range $R=R_C$	System	Dual
Aperture	a	a
Azimuthal Resolution	a	a
f-number	$f_{\#}$	$f_{\#}$
Angular Resolution	θ_R	θ_R
Depth of Focus	$\pm R_C$	$\pm R_C$
Near Field/Far Field Crossover	R_C	R_C

Summary

The geometrical relationships of this section, although approximate, are rules of thumb that all ultrasound engineers should know. They are applicable to virtually all modern diagnostic ultrasound systems, and yield insights into visible aspects of their performance.

Geometrical Optics Summary		
f-number	$f_{\#}$	R/a
Angular Resolution	θ_R	λ/a
Azimuthal Resolution	u_R	$f_{\#}\lambda$
Depth of Focus	r_D	$\pm f_{\#}^2\lambda$
Near Field/Far Field Crossover	R_C	a^2/λ

However, the geometrical approach is ultimately limited as an analytical tool for understanding many issues of critical interest. For example, do our compensating delays yield azimuthal resolution that is optimal in any sense? And how do we conceptualize the transformation between object and image? For these sorts of questions we turn to Fourier theory.

Linear Shift-Invariant Systems and Transforms

Representation of Signals in One Dimension[1,2,3]

In one dimension, we can expand a function several ways, but there are two canonical approaches.

Expansion of a Signal in Dirac Delta Functions

We can think of an idealized sample of a function $g(t)$ at time τ as

$$g(\tau)\delta(t-\tau) \tag{3.1}$$

Integrating these contributions we obtain the original signal

$$g(t) = \int_{-\infty}^{\infty} d\tau\, g(\tau)\delta(t-\tau) \tag{3.2}$$

by virtue of the characteristics of the delta function under integration. For a LSI system, knowing the impulse response $h(t)$ lets us infer the response for any input. Using the symbol $\Rightarrow$ to indicate the operation of a LSI system, with the input on the left and the output on the right, it follows that

$$\begin{aligned} \delta(t-\tau) &\Rightarrow h(t-\tau) \\ g(\tau)\delta(t-\tau) &\Rightarrow g(\tau)h(t-\tau) \\ \int_{-\infty}^{\infty} d\tau\, g(\tau)\delta(t-\tau) &\Rightarrow \int_{-\infty}^{\infty} d\tau\, g(\tau)h(t-\tau) \\ g(t) &\Rightarrow \int_{-\infty}^{\infty} d\tau\, g(\tau)h(t-\tau) \end{aligned} \tag{3.3}$$

In this way, we can think of the familiar convolution integral as the shifted, weighted superposition of impulse responses, in which the weights are the expansion coefficients of the input signal.

Expansion of a Signal in Complex Exponentials. The Fourier Transform

The Fourier transform expresses a signal $g(t)$ as an expansion of complex exponentials.

$$g(t) = \int_{-\infty}^{\infty} df\, G(f) \exp(j2\pi ft) \tag{3.4}$$

where

$$G(f) = \int_{-\infty}^{\infty} dt\, g(t) \exp(-j2\pi ft) \tag{3.5}$$

We refer to eq. (3.4) as the inverse Fourier transform and eq. (3.5) as the (forward) Fourier transform of the signal $g(t)$.

Complex exponentials are eigenfunctions of LSI systems; that is, if we excite such a system with a function of the form $\exp(j2\pi ft)$ then the output is of the form $H(f)\exp(j2\pi ft)$, where $H(f)$ is a complex weight dependent on *f* but independent of *t*. It follows that

$$\begin{aligned} \exp(j2\pi ft) &\Rightarrow H(f)\exp(j2\pi ft) \\ G(f)\exp(j2\pi ft) &\Rightarrow G(f)H(f)\exp(j2\pi ft) \\ \int_{-\infty}^{\infty} df\, G(f)\exp(j2\pi ft) &\Rightarrow \int_{-\infty}^{\infty} df\, G(f)H(f)\exp(j2\pi ft) \\ g(t) &\Rightarrow \int_{-\infty}^{\infty} df\, G(f)H(f)\exp(j2\pi ft) \end{aligned} \tag{3.6}$$

These two expansions, in the context of LSI systems, are duals of each other. If we take the Fourier transform of both sides of the first line of eq. (3.3)

$$\begin{aligned} \Im\{\delta(t-\tau)\} &\Rightarrow \Im\{h(t-\tau)\} \\ \exp(-j2\pi f\tau) &\Rightarrow H(f)\exp(-j2\pi f\tau) \end{aligned} \tag{3.7}$$

we get the first line of eq. (3.6) in its essentials. This is because shifted delta functions and complex exponentials are Fourier transform pairs.

Some Properties of Fourier Transforms in One Dimension

Let $h(t)$ and $H(f)$ be Fourier transform pairs, and their relationship represented with the symbol $\Leftrightarrow$; likewise $g(t)$ and $G(f)$. The operator $*$ represents one dimensional convolution.

Reversal/Conjugation

$$\begin{aligned} h(t) &\Leftrightarrow H(f) \\ h(-t) &\Leftrightarrow H(-f) \\ h^*(t) &\Leftrightarrow H^*(-f) \\ h^*(-t) &\Leftrightarrow H^*(f) \end{aligned} \tag{3.8}$$

Convolution/Multiplication

$$\begin{aligned} h(t) * g(t) &\Leftrightarrow H(f)\, G(f) \\ h(t)\, g(t) &\Leftrightarrow H(f) * G(f) \end{aligned} \tag{3.9}$$

Shift/Modulation

$$\begin{aligned} h(t-a) &\Leftrightarrow H(f)\, e^{-j2\pi af} \\ h(t)\, e^{j2\pi at} &\Leftrightarrow H(f-a) \end{aligned} \tag{3.10}$$

Power/Rayleigh's Theorem

$$\begin{aligned} \int_{-\infty}^{\infty} dt\; h(t)\, g^*(t) &= \int_{-\infty}^{\infty} df\; H(f)\, G^*(f) \\ \int_{-\infty}^{\infty} dt\; |h(t)|^2 &= \int_{-\infty}^{\infty} df\; |H(f)|^2 \end{aligned} \tag{3.11}$$

Definite Integral/Central Ordinate

$$\begin{aligned} \int_{-\infty}^{\infty} dt\; h(t) &= H(0) \\ h(0) &= \int_{-\infty}^{\infty} df\; H(f) \end{aligned} \tag{3.12}$$

Similarity

$$\begin{aligned} h\left(\frac{t}{a}\right) &\Leftrightarrow |a|\, H(af) \\ |a|\, h(at) &\Leftrightarrow H\left(\frac{f}{a}\right) \end{aligned} \tag{3.13}$$

The Multidimensional Fourier Transform[1,4,5]

Consider a multidimensional function represented in Cartesian coordinates as $h(x_1, x_2, \ldots x_n) = h(\mathbf{x})$. Its Fourier transform and its inverse are

$$\begin{aligned} H(\mathbf{u}) &= \int d\mathbf{x}\, h(\mathbf{x}) \exp(-j2\pi\, \mathbf{u}\cdot\mathbf{x}) \\ &= \int dx_1\, dx_2 \ldots dx_n\, h(x_1, x_2, \ldots x_n) \exp\left(-j2\pi\left[u_1 x_1 + u_2 x_2 + \ldots u_n x_n\right]\right) \end{aligned} \tag{3.14}$$

$$\begin{aligned} h(\mathbf{x}) &= \int d\mathbf{u}\, H(\mathbf{u}) \exp(j2\pi\, \mathbf{u}\cdot\mathbf{x}) \\ &= \int du_1\, du_2 \ldots du_n\, H(u_1, u_2, \ldots u_n) \exp\left(j2\pi\left[u_1 x_1 + u_2 x_2 + \ldots u_n x_n\right]\right) \end{aligned} \tag{3.15}$$

where the integrations are taken over all space.

We can view these integral relationships as straightforward extensions of the one-dimensional case. Here, a multidimensional function is expressed as an expansion of complex exponentials of the same dimensionality. Note that the function and its transform may represent a signal, or the impulse response of a multidimensional system.

Separability

Let $h(x_1, x_2, \ldots x_n)$ be separable, such that

$$h(x_1, x_2, \ldots x_n) = h_1(x_1, x_2, \ldots x_m)\, h_2(x_{m+1}, x_{m+2}, \ldots x_n) \tag{3.16}$$

Then its Fourier transform is similarly separable.

$$H(u_1, u_2, \ldots u_n) = H_1(u_1, u_2, \ldots u_m)\, H_2(u_{m+1}, u_{m+2}, \ldots u_n) \tag{3.17}$$

Rotational Symmetry

In the special case that $h(\mathbf{x})$ is rotationally symmetric, then $H(\mathbf{u})$ is likewise rotationally symmetric. Both are representations of one independent variable, even though the functions are multidimensional.

$$\begin{aligned} h(\mathbf{x}) &= \hat{h}(r) \quad ; \quad r = |\mathbf{x}| \\ H(\mathbf{u}) &= \hat{H}(s) \quad ; \quad s = |\mathbf{u}| \end{aligned} \tag{3.18}$$

The Hankel Transform of a Rotationally Symmetric Function

Under the special condition of rotational symmetry, the one dimensional Hankel transform is identically an n-dimensional Fourier transform. Using the notation of eq. (3.18), and where $J_n(\cdot)$ is the Bessel function of the first kind of order *n*, the transform for a rotationally symmetric function is

$$\hat{H}(s) = \frac{2\pi}{s^{\frac{n}{2}-1}} \int_0^\infty dr\, r^{\frac{n}{2}}\, \hat{h}(r)\, \mathrm{J}_{\frac{n}{2}-1}(2\pi sr) \tag{3.19}$$

$$\hat{h}(r) = \frac{2\pi}{r^{\frac{n}{2}-1}} \int_0^\infty ds\, s^{\frac{n}{2}}\, \hat{H}(s)\, \mathrm{J}_{\frac{n}{2}-1}(2\pi sr) \tag{3.20}$$

Radial Symmetry: The Hankel Transform of a Two Dimensional Function

Applying the above to a two-dimensional radially symmetric function, we get what is sometimes called the Fourier-Bessel transform.

$$\begin{aligned} h(x,y) &= \hat{h}(r) \quad ; \quad r = \sqrt{x^2 + y^2} \\ H(u,v) &= \hat{H}(s) \quad ; \quad s = \sqrt{u^2 + v^2} \end{aligned} \tag{3.21}$$

$$\hat{H}(s) = 2\pi \int_0^\infty dr\, r\, \hat{h}(r)\, \mathrm{J}_0(2\pi sr) \tag{3.22}$$

$$\hat{h}(r) = 2\pi \int_0^\infty ds\, s\, \hat{H}(s)\, \mathrm{J}_0(2\pi sr) \tag{3.23}$$

Spherical Symmetry: The Hankel Transform of a Three Dimensional Function

Applying the above to a three-dimensional spherically symmetric function yields

$$\begin{aligned} h(x,y,z) &= \hat{h}(r) \quad ; \quad r = \sqrt{x^2 + y^2 + z^2} \\ H(u,v,w) &= \hat{H}(s) \; ; \quad s = \sqrt{u^2 + v^2 + w^2} \end{aligned} \tag{3.24}$$

$$\hat{H}(s) = \frac{2}{s} \int_0^\infty dr\, r\, \hat{h}(r) \sin(2\pi sr) \tag{3.25}$$

$$\hat{h}(r) = \frac{2}{r} \int_0^\infty ds\, s\, \hat{H}(s) \sin(2\pi sr) \tag{3.26}$$

Some Properties of Fourier Transforms in Multiple Dimensions

Several elementary properties are easily derived from the transform definition, and are straightforward extensions of their one dimensional counterparts. The notation $\underset{n}{*}$ denotes n-dimensional convolution.

Reversal/Conjugation

$$\begin{aligned} h(\mathbf{x}) &\Leftrightarrow H(\mathbf{u}) \\ h(-\mathbf{x}) &\Leftrightarrow H(-\mathbf{u}) \\ h^*(\mathbf{x}) &\Leftrightarrow H^*(-\mathbf{u}) \\ h^*(-\mathbf{x}) &\Leftrightarrow H^*(\mathbf{u}) \end{aligned} \tag{3.27}$$

Convolution/Multiplication

$$\begin{aligned} h(\mathbf{x}) \underset{n}{*} g(\mathbf{x}) &\Leftrightarrow H(\mathbf{u})\, G(\mathbf{u}) \\ h(\mathbf{x})\, g(\mathbf{x}) &\Leftrightarrow H(\mathbf{u}) \underset{n}{*} G(\mathbf{u}) \end{aligned} \tag{3.28}$$

Shift/Modulation

$$\begin{aligned} h(\mathbf{x}-\mathbf{a}) &\Leftrightarrow H(\mathbf{u})\, e^{-j2\pi \mathbf{a}\cdot\mathbf{u}} \\ h(\mathbf{x})\, e^{j2\pi \mathbf{a}\cdot\mathbf{x}} &\Leftrightarrow H(\mathbf{u}-\mathbf{a}) \end{aligned} \tag{3.29}$$

Power/Rayleigh's Theorem

$$\begin{aligned} \int d\mathbf{x}\, h(\mathbf{x})\, g^*(\mathbf{x}) &= \int d\mathbf{u}\, H(\mathbf{u})\, G^*(\mathbf{u}) \\ \int d\mathbf{x}\, |h(\mathbf{x})|^2 &= \int d\mathbf{u}\, |H(\mathbf{u})|^2 \end{aligned} \tag{3.30}$$

Definite Integral/Central Ordinate

$$\begin{aligned} \int d\mathbf{x}\, h(\mathbf{x}) &= H(\mathbf{0}) \\ h(\mathbf{0}) &= \int d\mathbf{u}\, H(\mathbf{u}) \end{aligned} \tag{3.31}$$

Similarity

$$\begin{aligned} h\left(\frac{x_1}{a_1}, \frac{x_2}{a_2}, \ldots \frac{x_n}{a_n}\right) &\Leftrightarrow |a_1 a_2 \ldots a_n|\, H(a_1 u_1, a_2 u_2, \ldots a_n u_n) \\ |a_1 a_2 \ldots a_n|\, h(a_1 x_1, a_2 x_2, \ldots a_n x_n) &\Leftrightarrow H\left(\frac{u_1}{a_1}, \frac{u_2}{a_2}, \ldots \frac{u_n}{a_n}\right) \end{aligned} \tag{3.32}$$

Marginal Fourier Transforms in Multiple Dimensions

It is often useful in multidimensional Fourier analysis to transform with respect to some of the independent variables but not all of them. In so doing we obtain a marginal transform. The properties of marginal transforms extend simply from the properties of full transforms, and are easily derived. We illustrate here with a two-dimensional example.

$$\begin{aligned} H_x(u,y) &= \int_{-\infty}^{\infty} dx\, h(x,y)\exp(-j2\pi ux) \\ h(x,y) &= \int_{-\infty}^{\infty} du\, H_x(u,y)\exp(j2\pi ux) \end{aligned} \tag{3.33}$$

We augment our $\Leftrightarrow$ notation to represent the marginal transform relationship.

$$h(x,y) \underset{x}{\Leftrightarrow} H_x(u,y) \tag{3.34}$$

The most important properties include:

Convolution

$$h(x,y) \underset{x,y}{*} g(x,y) \underset{x}{\Leftrightarrow} H_x(u,y) \underset{y}{*} G_x(u,y) \tag{3.35}$$

Power

$$\int_{-\infty}^{\infty} dx \int_{-\infty}^{\infty} dy\, h(x,y)\, g^*(x,y) = \int_{-\infty}^{\infty} du \int_{-\infty}^{\infty} dy\, H_x(u,y)\, G_x^*(u,y) \tag{3.36}$$

Definite Integral

$$\int_{-\infty}^{\infty} dx\, h(x,y) = H_x(0,y) \tag{3.37}$$

Multidimensional Fourier Transforms in Space and Time; Plane Waves

In working with four dimensional functions of space and time, we will use x, y, z as the spatial variables, u, v, w as the corresponding spatial frequency variables, t as the temporal variable, and f as the corresponding temporal frequency variable. As appropriate, we will also use the vector notation $\mathbf{x}$ and $\mathbf{u}$. The transform pairs are thus

$$\begin{aligned} h(x,y,z,t) &= \int_{-\infty}^{\infty} du \int_{-\infty}^{\infty} dv \int_{-\infty}^{\infty} dw \int_{-\infty}^{\infty} df\ H(u,v,w,f) \exp\left(j2\pi\left[ux+vy+wz+ft\right]\right) \\ H(u,v,w,f) &= \int_{-\infty}^{\infty} dx \int_{-\infty}^{\infty} dy \int_{-\infty}^{\infty} dz \int_{-\infty}^{\infty} dt\ h(x,y,z,t) \exp\left(-j2\pi\left[ux+vy+wz+ft\right]\right) \end{aligned} \tag{3.38}$$

or, equivalently

$$\begin{aligned} h(\mathbf{x},t) &= \int d\mathbf{u} \int_{-\infty}^{\infty} df\ H(\mathbf{u},f) \exp\left(j2\pi\left[\mathbf{u}\cdot\mathbf{x}+ft\right]\right) \\ H(\mathbf{u},f) &= \int d\mathbf{x} \int_{-\infty}^{\infty} dt\ h(\mathbf{x},t) \exp\left(-j2\pi\left[\mathbf{u}\cdot\mathbf{x}+ft\right]\right) \end{aligned} \tag{3.39}$$

The Fourier kernel $\exp\left(\pm j2\pi\left[ux+vy+wz+ft\right]\right)$ is a plane wave, so a transform represents a function as an expansion of complex plane waves. Of course, not all plane waves will propagate in a medium—only those whose spatial wavelength and temporal frequency are related by the propagation velocity of the medium.

The Multidimensional Dirac Delta Function

As a simple extension of the one-dimensional case, the multidimensional Dirac delta function also has the sifting property. Using vector notation

$$h(\mathbf{x}_0) = \int d\mathbf{x}\, h(\mathbf{x})\ {}^n\delta(\mathbf{x_0} - \mathbf{x}) \tag{3.40}$$

It also has a similar Fourier transform relationship

$${}^n\delta(\mathbf{x} - \mathbf{x_0}) \Leftrightarrow \exp(-j2\pi\, \mathbf{u} \cdot \mathbf{x_0}) \tag{3.41}$$

To help secure some of the notation for the course, these relationships can be expressed in four dimensions of space and time. The sifting property of eq. (3.40) thus becomes

$$h(x_0, y_0, z_0, t_0) = \int_{-\infty}^{\infty} dx \int_{-\infty}^{\infty} dy \int_{-\infty}^{\infty} dz \int_{-\infty}^{\infty} dt\ h(x, y, z, t)\ {}^4\delta(x_0 - x,\, y_0 - y,\, z_0 - z,\, t_0 - t) \tag{3.42}$$

and the forward and inverse transforms of eq. (3.41) becomes

$$\begin{aligned} &{}^4\delta(x - x_0, y - y_0, z - z_0, t - t_0) = \\ &\quad \int_{-\infty}^{\infty} du \int_{-\infty}^{\infty} dv \int_{-\infty}^{\infty} dw \int_{-\infty}^{\infty} df\ \exp(-j2\pi[ux_0 + vy_0 + wz_0 + ft_0]) \exp(j2\pi[ux + vy + wz + ft]) \end{aligned} \tag{3.43}$$

$$\begin{aligned} &\exp(-j2\pi[ux_0 + vy_0 + wz_0 + ft_0]) = \\ &\quad \int_{-\infty}^{\infty} dx \int_{-\infty}^{\infty} dy \int_{-\infty}^{\infty} dz \int_{-\infty}^{\infty} dt\ {}^4\delta(x - x_0, y - y_0, z - z_0, t - t_0) \exp(-j2\pi[ux + vy + wz + ft]) \end{aligned}$$

Expressed in all their glory, these relationships can appear quite intimidating (which is one good reason for resorting to vector notation). Its important to keep in mind that these relationships are, in fact, no more complex than their familiar one-dimensional counterparts, and that one should always focus on the underlying geometry of the problem, as it is often simpler than its analytical expression.

Acoustic Propagation and Reflection

The Scalar Wave Equation

The driven scalar wave equation governing the propagation of energy in an idealized medium is

$$\nabla^2\phi(x,y,z,t) - \frac{1}{c_0^2}\frac{\partial^2}{\partial t^2}\phi(x,y,z,t) = \psi(x,y,z,t) \tag{4.1}$$

The scalar $\phi(x,y,z,t)$ is usually taken to be pressure or the velocity potential, and $\psi(x,y,z,t)$ is the driving function. Taking the marginal Fourier transform with respect to time yields the Helmholtz equation

$$\nabla^2\phi_f(x,y,z,f) + \frac{4\pi^2 f^2}{c_0^2}\phi_f(x,y,z,f) = \psi_f(x,y,z,f) \tag{4.2}$$

Propagation Velocity and Losses[6]

A commonly accepted idealized velocity of propagation for diagnostic ultrasound is 1540 *m/s*. Adding viscosity to the medium introduces losses that are small but non-negligible. A common (and quite rigorous) technique for introducing this effect analytically is to define the velocity of propagation as a complex quantity, dependent on the frequency *f* and conjugate symmetric over *f*. The simplest model for diagnostic ultrasound is

$$\frac{1}{c} = \begin{cases} \frac{1}{c_0}(1 - j\alpha) & ; \quad f > 0 \\ \frac{1}{c_0} & ; \quad f = 0 \\ \frac{1}{c_0}(1 + j\alpha) & ; \quad f < 0 \end{cases} \tag{4.3}$$

where c_0 is real and $\alpha \geq 0$ is the loss tangent of the medium. The conjugate symmetry ensures that a real forcing function $\psi(x,y,z,t)$ will excite a real propagating function $\phi(x,y,z,t)$. The Helmholtz equation thus becomes

$$\nabla^2\phi_f(x,y,z,f) + \frac{4\pi^2 f^2}{c^2}\phi_f(x,y,z,f) = \psi_f(x,y,z,f) \tag{4.4}$$

For soft biological tissue in the frequency range commonly used in diagnostic ultrasound, a useful approximation is $\alpha \cong 3\times 10^{-3}$.

Propagation as a Linear Shift Invariant System[7]

The scalar wave equation is linear and shift invariant in both time and space. We can think of acoustic propagation as a LSI system, and use multidimensional Fourier techniques for analysis, insight, and inspiration.

In taking the approach to follow, we make a number of important simplifying assumptions:

- The propagation medium is homogeneous
- The only non-negligible boundary condition is the forcing function
- The only scattering is low-level

It is certainly easy to find specific imaging situations where one or more of these assumptions are violated, but the success of diagnostic ultrasound is evidence of their general applicability. More importantly, deep understanding of the simple cases will afford insights into the more complex ones.

Following the development we used for the one-dimensional LSI case, we argue that knowledge of the impulse response $g(x,y,z,t)$ or the transfer function $G(u,v,w,f)$ (which are Fourier transform pairs) of propagation in the medium of interest will let us characterize the response to any spatio-temporal input.

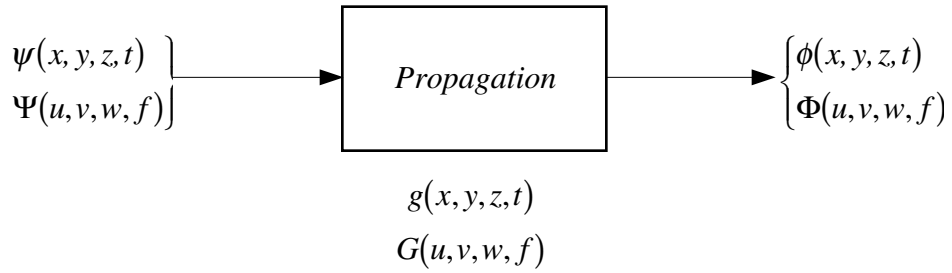

(4.5)

Let us start by considering the lossy Helmholtz equation. If the forcing function is a four-dimensional delta function in time and space, the marginal transformation to temporal frequency results in a three-dimensional delta function. By definition, the output in this case is the marginal impulse response $g_f(x,y,z,f)$.

$$\nabla^2 g_f(x,y,z,f) + \frac{4\pi^2 f^2}{c^2} g_f(x,y,z,f) = {}^3\delta(x,y,z) \tag{4.6}$$

Taking the three-dimensional Fourier transform of each side yields

$$\left(-4\pi^2u^2 - 4\pi^2v^2 - 4\pi^2w^2\right)G(u,v,w,f) + 4\pi^2\left(\frac{f}{c}\right)^2 G(u,v,w,f) = 1 \tag{4.7}$$

Recognizing the spherical symmetry, we let $s^2 = u^2 + v^2 + w^2$, which yields

$$\boxed{G(s,f) = \frac{1}{4\pi^2\left[\left(\frac{f}{c}\right)^2 - s^2\right]}} \tag{4.8}$$

It follows that the marginal transform $g_f(x,y,z,f)$ will also exhibit spherical symmetry, so we can use the inverse Hankel transform for three dimensions, eq. (3.26).

$$g_f(r,f) = \frac{2}{r}\int_0^\infty ds\; s\; G(s,f)\sin(2\pi sr) \tag{4.9}$$

Formal convergence of this integral occurs only for f/c having an imaginary component, thus moving the poles of $G(s,f)$ away from the real axis in the complex f plane. This represents a loss mechanism in any realizable system, and we use eq. (4.3) in this development to model it. Eq. (4.9) can then be evaluated using contour integration.

$$\boxed{\begin{aligned} g_f(r,f) &= -\frac{\exp\left(-j2\pi\frac{f}{c}r\right)}{4\pi r} \\ &= -\frac{\exp\left(-j2\pi\frac{f}{c_0}r\right)}{4\pi r}\cdot\exp\left(-2\pi|f|\alpha r/c_0\right) \end{aligned}} \tag{4.10}$$

This model thus presents a separable term $\exp\left(-2\pi|f|\alpha r/c_0\right)$ representing the loss of the system. This corresponds to about 55α dB/wavelength; when $\alpha = 3\times10^{-3}$, the loss is about 1dB/cm MHz, a commonly reported value in diagnostic imaging.

Taking the inverse Fourier transform on eq. (4.10) yields the impulse response of the propagating medium represented by the scalar wave equation.

$$\boxed{g(r,t) = -\frac{\delta(t - r/c_0)}{4\pi r} *_t \frac{1}{\pi}\left[\frac{(\alpha r/c_0)}{(\alpha r/c_0)^2 + t^2}\right]} \tag{4.11}$$

We refer to the second function as an attenuation filter. Using the definite integral property of Fourier transforms, we see that the area under the attenuation filter is unity, regardless of α. It similarly follows from Fourier considerations that

$$\lim_{\alpha r\to 0}\frac{1}{\pi}\left[\frac{(\alpha r/c_0)}{(\alpha r/c_0)^2 + t^2}\right] = \delta(t) \tag{4.12}$$

Thus in the limit of negligible loss

$$\boxed{g(r,t) = -\frac{\delta(t - r/c_0)}{4\pi r}} \tag{4.13}$$

This impulse response is often referred to as the free space Green's function. Note that it exists only for $t \geq 0$, this causality arising from the loss mechanism we introduced.

Having argued that propagation loss can be modeled as a linear filter in space and time, let us set the issue of loss aside and consider the underlying characteristics of lossless propagation. Note that eq. (4.13) is four dimensional, implying that, in addition to its Fourier transform, there are a total of fourteen marginal transforms. Spherical symmetry makes all but six of these redundant, and it is instructive to organize them in a cycle.

In the tables below, time and space are the variables in the lower right, and temporal frequency and spatial frequency occupy the upper left. Each function has as its neighbors its marginal transform taken with respect to one independent variable. The second table is the same as the first, but with the equations normalized for greater simplicity.

This cycle is not intended to model a particular medium, but rather to abstract out the process of propagation so we can consider it in its essentials. Indeed, these relationships exist only as mathematical abstractions; there is no way to generate an acoustic impulse, nor is there any medium that can support one. However, when applied as convolution kernels and filter operators, these functions have all the familiar power of impulse responses and transfer functions.

The Fourier Transform Cycle of Ideal Propagation

$G(s,f) = \dfrac{1}{4\pi^2\left[\left(\dfrac{f}{c_0}\right)^2 - s^2\right]} + j\dfrac{\delta\left(s - \left\lvert\dfrac{f}{c_0}\right\rvert\right)}{8\pi\dfrac{f}{c_0}}$	$G_t(s,t) = -\dfrac{c_0 \sin(2\pi c_0 s t)}{2\pi s}\mu(t)$
$G_z(\hat{s},z,f) = \dfrac{j\exp\left\{-j2\pi\dfrac{f}{c_0}\lvert z\rvert\sqrt{1-\left(\dfrac{\hat{s}c_0}{f}\right)^2}\right\}}{4\pi\dfrac{f}{c_0}\sqrt{1-\left(\dfrac{\hat{s}c_0}{f}\right)^2}}$	$G_{z,t}(\hat{s},z,t) = -\dfrac{c_0\,\mathrm{J}_0\left\{2\pi c_0\hat{s}t\sqrt{1-\left(\dfrac{z}{c_0 t}\right)^2}\right\}}{2}\mathrm{rect}\left(\dfrac{z}{2c_0 t}\right)\mu(t)$
$g_{u,f}(\tilde{r},u,f) = -\dfrac{\mathrm{K}_0\left\{j2\pi\dfrac{f}{c_0}\tilde{r}\sqrt{1-\left(\dfrac{uc_0}{f}\right)^2}\right\}}{2\pi}$	$g_u(\tilde{r},u,t) = -\dfrac{\cos\left\{2\pi c_0 u t\sqrt{1-\left(\dfrac{\tilde{r}}{c_0 t}\right)^2}\right\}}{2\pi t\sqrt{1-\left(\dfrac{\tilde{r}}{c_0 t}\right)^2}}\mathrm{rect}\left(\dfrac{\tilde{r}}{2c_0 t}\right)\mu(t)$
$g_f(r,f) = -\dfrac{\exp\left(-j2\pi\dfrac{f}{c_0}r\right)}{4\pi r}$	$g(r,t) = -\dfrac{\delta\left(t-\dfrac{r}{c_0}\right)}{4\pi r}$

Notes

- This is the causal impulse response of the lossless scalar wave equation.
- In the evanescent regime, the real part of $\left\{-j2\pi\dfrac{f}{c_0}\lvert z\rvert\sqrt{1-\left(\dfrac{\hat{s}c_0}{f}\right)^2}\right\}$ and of $\left\{j2\pi\dfrac{f}{c_0}\tilde{r}\sqrt{1-\left(\dfrac{uc_0}{f}\right)^2}\right\}$ are positive.
- The function $\delta(\cdot)$ is the Dirac delta function. The function $\mu(\cdot)$ is the Heaviside step function. $\mathrm{J}_0(\cdot)$ is the Bessel function of the first kind, order zero. $\mathrm{K}_0(\cdot)$ is the modified Bessel function of the second kind, order zero.
- $r^2 = x^2 + y^2 + z^2$
- $s^2 = u^2 + v^2 + w^2$
- $\tilde{r}^2 = y^2 + z^2$
- $\hat{s}^2 = u^2 + v^2$

The Normalized Fourier Transform Cycle of Ideal Propagation

$G\left(s,\hat{f}\right)=\frac{1}{4\pi^2\left[\hat{f}^2-s^2\right]}+j\frac{\delta\left(s-\left\|\hat{f}\right\|\right)}{8\pi\hat{f}}$	$\hat{G}_t\left(s,\hat{t}\right)=-\frac{\sin\left(2\pi s\hat{t}\right)}{2\pi s}\mu\left(\hat{t}\right)$
$G_z\left(\hat{s},z,\hat{f}\right)=\frac{j\exp\left\{-j2\pi\hat{f}\left\|z\right\|\sqrt{1-\left(\frac{\hat{s}}{\hat{f}}\right)^2}\right\}}{4\pi\hat{f}\sqrt{1-\left(\frac{\hat{s}}{\hat{f}}\right)^2}}$	$\hat{G}_{z,t}\left(\hat{s},z,\hat{t}\right)=-\frac{\mathrm{J}_0\left\{2\pi\hat{s}\hat{t}\sqrt{1-\left(\frac{z}{\hat{t}}\right)^2}\right\}}{2}\mathrm{rect}\left(\frac{z}{2\hat{t}}\right)\mu\left(\hat{t}\right)$
$g_{u,f}\left(\tilde{r},u,\hat{f}\right)=-\frac{\mathrm{K}_0\left\{j2\pi\hat{f}\tilde{r}\sqrt{1-\left(\frac{u}{\hat{f}}\right)^2}\right\}}{2\pi}$	$\hat{g}_u\left(\tilde{r},u,\hat{t}\right)=-\frac{\cos\left\{2\pi u\hat{t}\sqrt{1-\left(\frac{\tilde{r}}{\hat{t}}\right)^2}\right\}}{2\pi\hat{t}\sqrt{1-\left(\frac{\tilde{r}}{\hat{t}}\right)^2}}\mathrm{rect}\left(\frac{\tilde{r}}{2\hat{t}}\right)\mu\left(\hat{t}\right)$
$g_f\left(r,\hat{f}\right)=-\frac{\exp\left(-j2\pi\hat{f}r\right)}{4\pi r}$	$\hat{g}\left(r,\hat{t}\right)=-\frac{\delta\left(\hat{t}-r\right)}{4\pi r}$

Notes

- The Fourier cycle is normalized such that $\hat{f}=\frac{f}{c_0}$ and $\hat{t}=c_0t,$ and the similarity theorem applied.
- In the evanescent regime, the real part of $\left\{-j2\pi\hat{f}\left\|z\right\|\sqrt{1-\left(\frac{\hat{s}}{\hat{f}}\right)^2}\right\}$ and of $\left\{j2\pi\hat{f}\tilde{r}\sqrt{1-\left(\frac{u}{\hat{f}}\right)^2}\right\}$ are positive.
- The function $\delta(\cdot)$ is the Dirac delta function. The function $\mu(\cdot)$ is the Heaviside step function. $\mathrm{J}_0(\cdot)$ is the Bessel function of the first kind, order zero. $\mathrm{K}_0(\cdot)$ is the modified Bessel function of the second kind, order zero.
- $r^2=x^2+y^2+z^2$
- $s^2=u^2+v^2+w^2$
- $\tilde{r}^2=y^2+z^2$
- $\hat{s}^2=u^2+v^2$

Low-Level Scattering[8]

Consider an illumination wavefield $\gamma(x,y,z,t)$ propagating in a medium containing a discontinuity of arbitrarily small dimensions at location x_0, y_0, z_0. The discontinuity will induce a scattered wavefield $\phi(x,y,z,t|x_0,y_0,z_0)$ that will appear as originating from a point source of the form

$$\psi(x,y,z,t|x_0,y_0,z_0) = \gamma(x_0,y_0,z_0,t) *_t o(x_0,y_0,z_0,t)^3 \delta(x-x_0, y-y_0, z-z_0) \tag{4.14}$$

That is, our point discontinuity becomes an induced source, radiating a weighted and temporally filtered version of its illumination. The resulting scattered wavefield is simply the convolution of the induced point source $\psi(\cdot)$ with the impulse response (i.e., the free space Green's function) $g(\cdot)$

$$\phi(x,y,z,t|x_0,y_0,z_0) = \gamma(x_0,y_0,z_0,t) *_t o(x_0,y_0,z_0,t) *_t g(x-x_0, y-y_0, z-z_0, t) \tag{4.15}$$

Low-level scattering is the assumption that the illumination wavefield is substantially unchanged by the presence of scatters and scattering. In that case, we can associate a distinct weight $o(x_0,y_0,z_0,t)$ to every point in space and superpose the distinct responses. The total scattered wavefield is

$$\begin{aligned} \phi(x,y,z,t) &= \int dx_0 \int dy_0 \int dz_0 \; \phi(x,y,z,t|x_0,y_0,z_0) \\ &= \int dx_0 \int dy_0 \int dz_0 \; \gamma(x_0,y_0,z_0,t) *_t o(x_0,y_0,z_0,t) *_t g(x-x_0, y-y_0, z-z_0, t) \end{aligned} \tag{4.16}$$

whence

$$\phi(x,y,z,t) = \left[\gamma(x,y,z,t) *_t o(x,y,z,t)\right] *_{x,y,z,t} g(x,y,z,t) \tag{4.17}$$

In this formulation, the object field $o(x,y,z,t)$ is a four-dimensional entity representing acoustic reflectivity under the assumption of low-level scattering. The challenge of acoustic imaging is to come up with a representation of the object field, generally in two dimensions, that has utility.

We may use various marginal transforms on eq. (4.17) for different perspectives on the process. Taking the marginal transform with respect to time yields

$$\phi_f(x,y,z,f) = \left[\gamma_f(x,y,z,f)\, o_f(x,y,z,f)\right] \underset{x,y,z}{*} g_f(x,y,z,f) \tag{4.18}$$

To see how this particular relationship might be used, consider the problem of determining the scattered response at a single point in space (where we might have a small transducer); without loss of generality let our receiver point be the origin. Then eq. (4.18) becomes

$$\phi_f(0,0,0,f) = \int dx \int dy \int dz\, \gamma_f(x,y,z,f)\, o_f(x,y,z,f)\, g_f(x,y,z,f) \tag{4.19}$$

Taking a further marginal transform with respect to *x* and *y*

$$\Phi_z(u,v,z,f) = \left[\Gamma_z(u,v,z,f) \underset{u,v}{*} O_z(u,v,z,f)\right] \underset{z}{*} G_z(u,v,z,f) \tag{4.20}$$

Suppose we have a planar receive aperture in the plane *z=0*. Eq. (4.20) reduces to

$$\Phi_z(u,v,0,f) = \int dz \left[\Gamma_z(u,v,z,f) \underset{u,v}{*} O_z(u,v,z,f)\right] G_z(u,v,z,f) \tag{4.21}$$

Acoustic Sources, Sensors, and Boundary Conditions[7]

The transmission (and the reciprocal process, reception) of acoustic signals requires transducers coupled to the propagation medium. Their transfer function is the subject of scalar diffraction theory. Recall that Green's theorem and the Sommerfeld radiation condition lead to the following integral equation

$$\phi_f(x,y,z,f) = \int_{-\infty}^{\infty} dx \int_{-\infty}^{\infty} dy \left[\frac{\partial \phi_f}{\partial n} \Gamma_f - \phi_f \frac{\partial \Gamma_f}{\partial n} \right] \tag{4.22}$$

describing radiation from a source in the plane $z=0$. Here Γ_f is an artfully chosen Green's function and $\partial/\partial n$ is the spatial derivative normal to the transducer plane, i.e., in the z direction. Two Rayleigh-Sommerfeld canonical equations, derived using two different Green's functions, are well-known. We write them here as two dimensional convolutions, and use pressure as the scalar field function.

$$p_f(x,y,z,f) = \left[2 \frac{\partial p_f(x,y,z,f)}{\partial z} \right]_{z=0} \underset{x,y}{*} \left[-\frac{\exp\left(-j2\pi \frac{f}{c_0} r \right)}{4\pi r} \right] \tag{4.23}$$

$$p_f(x,y,z,f) = \left[2 p_f(x,y,0,f) \right] \underset{x,y}{*} \left[-\frac{\exp\left(-j2\pi \frac{f}{c_0} r \right)}{4\pi r} \cdot \frac{z}{r} \left(\frac{1 + j2\pi f r/c_0}{r} \right) \right] \tag{4.24}$$

(Note that corresponding expressions in the literature often have an inconsequential reversal of the sign of f.)

The two equations are, of course, equally valid. The choice of one expression or the other in a specific application is usually governed by convenient assumptions about the characteristics of the planar surface from which the signal is transmitted[9], or by the need to match empirical data.[10]

Specifically, consider the case of a rigid plane, such that the normal derivative of pressure (proportional to the temporal derivative of the normal velocity) is zero beyond the physical limits of the forcing function. Then the natural expression to use is eq. (4.23), and the resulting convolution limits are the physical limits of the forcing function. In this case, the forcing function is usually the temporal derivative of the normal velocity at the transducer face.

Alternatively, consider the plane of interest as a pressure release surface, on which the pressure is zero beyond the physical limits of the forcing function. Then eq. (4.24) is the more natural choice, and the forcing function is the pressure at the transducer face.

For our subsequent development we will always use eq. (4.23), because the *convolution kernel is the free space Green's function*. This *unifies our approach to propagation, scattering, transmission, and reception*.

In so doing we make no assumptions about the impedance of the transducer plane, but rather recognize that the driving function will not, in general, be bound by the physical dimensions of the transducer. To be more specific on the last point, imagine an array of transducer elements in the plane $z=0$. For any one element driven electrically with a unit-amplitude complex sinusoid with frequency f, we can associate some elemental function $w(x, y, f)$ that will serve in the Rayleigh-Sommerfeld convolution integral of eq. (4.23). This association depends on the details of the transducer design, and will be knowable empirically if not theoretically. Any realizable aperture function will then be comprised of weighted sums of these elemental functions.

Backpropagation and the Angular Spectrum[7,11]

Consider the lossless Helmholtz equation in a region of space which includes no sources.

$$\nabla^2\phi_f(x,y,z,f)+\frac{4\pi^2 f^2}{c_0^2}\phi_f(x,y,z,f)=0 \tag{4.25}$$

We know that this equation is satisfied by any plane wave of the form

$$\exp\left(j2\pi[ux+vy+wz+ft]\right) \quad ; \quad u^2+v^2+w^2=\left(\frac{f}{c_0}\right)^2 \tag{4.26}$$

The terms $\left\{\frac{uc_0}{f},\frac{vc_0}{f},\frac{wc_0}{f}\right\}$ are the direction cosines, specifying the direction of propagation. When the sign of *w* and *f* are the same, propagation is in the negative *z* direction; when the same sign of *w* and *f* are opposite, propagation is in the positive *z* direction.

We want to know the wavefield $\phi(\cdot)$ in an arbitrary plane parallel to *z=0* given knowledge of it in the plane *z=0* (perhaps by measuring it with a planar array). If we take the marginal transform of eq. (4.25) with respect to *x* and *y* we get

$$\frac{\partial^2}{\partial z^2}\Phi_z(u,v,z,f)+\left[-4\pi^2u^2-4\pi^2v^2+\frac{4\pi^2f^2}{c_0^2}\right]\Phi_z(u,v,z,f)=0 \tag{4.27}$$

The general solution to this is straightforward. Recognizing the radial symmetry, we substitute $\hat{s}^2=u^2+v^2$.

$$\Phi_z(u,v,z,f)=A\exp\left\{j2\pi\frac{f}{c_0}z\sqrt{1-\left(\frac{\hat{s}c_0}{f}\right)}\right\}+B\exp\left\{-j2\pi\frac{f}{c_0}z\sqrt{1-\left(\frac{\hat{s}c_0}{f}\right)}\right\} \tag{4.28}$$

The first term corresponds to waves propagating in the negative *z* direction, and the second term to the positive *z* direction. This can be demonstrated by taking the Fourier transform of both sides; the right side of the equation will consist of two delta functions, the first constraining *w* to be the same sign as *f*, and the second constraining *w* to be the opposite sign as *f*. Hence our solution is

$$\frac{\Phi_z(u,v,z,f)}{\Phi_z(u,v,0,f)} = \begin{cases} \exp\left\{ j2\pi \frac{f}{c_0} z \sqrt{1-\left(\frac{\hat{s}c_0}{f}\right)} \right\} & ; \quad \text{propagation towards negative z} \\ \exp\left\{ -j2\pi \frac{f}{c_0} z \sqrt{1-\left(\frac{\hat{s}c_0}{f}\right)} \right\} & ; \quad \text{propagation towards positive z} \end{cases} \tag{4.29}$$

This a fascinating result. It says that if we have knowledge of a wavefield (and its direction of propagation relative to the z axis) at $z=0$, and we characterize the wavefield in terms of its two spatial frequencies and one temporal frequency, then we can determine the wavefield on any parallel plane, thus all (source-free) space. That is, one of the dimensions of the four dimensional representation of the wavefield is redundant by virtue of the wave equation.

The propagation filter $\exp\left\{ j2\pi \frac{f}{c_0} z \sqrt{1-\left(\frac{\hat{s}c_0}{f}\right)} \right\}$ is often used for backpropagation; that is, we characterize (perhaps measure) at $z=0$ a wavefield originating in positive half space and multiply by this filter to determine the wavefield at an earlier time and a greater distance. The filter is dispersive (non-linear phase) and all-pass up for $\hat{s} \le |f/c_0|$. We refer to this regime as the propagation regime. For $\hat{s} > |f/c_0|$ the exponent becomes negative real, and the amplitude rolls off extremely quickly. This regime is the evanescent regime. In most practical applications, the response in the evanescent regime is neglected.

The Pulse Echo Equation for a Fixed Focus Planar Transducer

Let's put all this together. Consider an imaging system consisting of a planar transmission aperture excited by a pulse, illuminating an object field consisting of low-level scatterers, and a planar reception aperture followed by a filter.

The pulse echo equation can be formulated with a distinct beamformation perspective, in that the transmission and reception apertures are specified with weights $w_t(x,y,f)$ and $w_r(x,y,f)$ respectively. We consider $w_t(x,y,f)$ and $w_r(x,y,f)$ fixed.

Illumination Wavefield

$$\gamma_f(x,y,z,f) = H_t(f)\, w_t(x,y,f) \underset{x,y}{*} g_f(x,y,z,f) \tag{4.30}$$

Reflected Wavefield

$$\phi_f(x,y,z,f) = \left[\gamma_f(x,y,z,f)\, o_f(x,y,z,f)\right] \underset{x,y,z}{*} g_f(x,y,z,f) \tag{4.31}$$

Sensed Wavefield

$$\phi_f(x,y,0,f) = \left[\left[\gamma_f(x,y,z,f)\, o_f(x,y,z,f)\right] \underset{x,y,z}{*} g_f(x,y,z,f)\right]_{z=0} \tag{4.32}$$

Received Signal

$$R(f) = H_r(f) \int dx \int dy\; w_r(x,y,f)\, \phi_f(x,y,0,f) \tag{4.33}$$

The Pulse Echo Equation

Making the substitutions and denoting $H_r(f)H_t(f) = H_{rt}(f)$ yields

$$R(f) = H_{rt}(f) \int dx \int dy \int dz\; o_f(x,y,z,f) \left[w_r(x,y,f) \underset{x,y}{*} g_f(x,y,z,f)\right]\left[w_t(x,y,f) \underset{x,y}{*} g_f(x,y,z,f)\right] \tag{4.34}$$

Eq. (4.34) can be rewritten simply as

$$\boxed{R_f(f) = \int dx \int dy \int dz\; o_f(x,y,z,f)\, s_f(x,y,z,f)} \tag{4.35}$$

where

$$\boxed{s_f(x,y,z,f) = H_{rt}(f)\left[w_r(x,y,f) \underset{x,y}{*} g_f(x,y,z,f)\right]\left[w_t(x,y,f) \underset{x,y}{*} g_f(x,y,z,f)\right]} \tag{4.36}$$

This last equation is an expression of the response of the system to a spatial impulse at location *x,y,z*. There are three simple components to $s_f(x,y,z,f)$.

- $H_{rt}(f)$: The round-trip pulse, in the temporal frequency domain.
- $\left[w_t(x,y,f) \underset{x,y}{*} g_f(x,y,z,f) \right]$: The wavefield associated with transmission.
- $\left[w_r(x,y,f) \underset{x,y}{*} g_f(x,y,z,f) \right]$: The spatial sensitivity associated with reception.

This expression of the pulse-echo response is quite general, and can be used as the basis for analyzing a wide variety of acoustic imaging systems, including synthetic aperture, fixed-focus lenses, dynamic-focus beamformers, and others. We will use it as the basis for our study of beamformer-based imaging systems.

In this context, we see the latter two components of $s_f(x,y,z,f)$ as identical formulations of one-way beamformation. In the next section we take a look at one-way beamformation to gain some insight into the appropriate aperture weights to use.

One-Way Beamformation and Spatial Filtering

Ultrasonic beamformation for diagnostic imaging is first a science, and ultimately an art. We will explore some of the former aspects of beamformation with the goal of providing context and inspiration for the latter. We start by considering the problem of one-way beamformation, with the goal of imaging a point source.

Reception Beamformation as Matched Filtering

Consider a point source, real or induced, at x_0, y_0, z_0 that transmits or scatters a signal $h_t(t)$. The resulting wavefield will be

$$\phi(x,y,z,t) = \left[h_t(t)\ {}^3\delta(x-x_0, y-y_0, z-z_0)\right] \underset{x,y,z,t}{*} g(x,y,z,t) \tag{5.1}$$

or, taking the marginal Fourier transform with respect to time and using vector notation

$$\phi_f(\mathbf{x}, f) = H_t(f)\left[-\frac{\exp\left(-j2\pi f\left|\mathbf{x}-\mathbf{x_0}\right|/c_0\right)}{4\pi\left|\mathbf{x}-\mathbf{x_0}\right|}\right] \tag{5.2}$$

Assume we have an array of sensors, or an aperture that lets us sense the wavefield at some locations in space. Further assume that each sensor or incremental portion of the aperture introduces additive uncorrelated white noise to the signal representing the sensed wavefield. We can pose the following problem. Given the sensor locations and the wavefield of eq. (5.1), determine the optimum spatio-temporal linear filter to maximize the signal-to-noise ratio (SNR) at filter output $(x,y,z,t) = (x_0, y_0, z_0, 0)$.

Denote the impulse response of the candidate filter $a^M(x,y,z,t)$. The convolution integral corresponding to the point for which we want to maximize the SNR is

$$\begin{aligned}\left[\phi(\mathbf{x},t) \underset{x,y,z,t}{*} a^M(\mathbf{x},t)\right]_{\mathbf{x_0},0} &= \int d\mathbf{x} \int dt\ \phi(\mathbf{x},t)\, a^M(\mathbf{x_0}-\mathbf{x}, -t) \\ &= \int d\mathbf{x} \int df\ \phi_f(\mathbf{x},f)\, a_f^M(\mathbf{x_0}-\mathbf{x}, f)\end{aligned} \tag{5.3}$$

where the spatial integration is taken over the location of the sensors. This is simply the multidimensional form of the matched filter problem. Using Schwartz' inequality and the characteristics of the additive noise, it follows that SNR is maximized when, within an arbitrary scale factor,

$$a_f^M(\mathbf{x_0}-\mathbf{x}, f) = \phi_f^*(\mathbf{x}, f) \tag{5.4}$$

whence

$$\boxed{a_f^M(\mathbf{x},f) = -H_t^*(f)\,\frac{\exp\left(j2\pi f|\mathbf{x}|/c_0\right)}{4\pi|\mathbf{x}|}} \tag{5.5}$$

If we interpret eq. (5.3) as the recipe for forming a beam at the point $\mathbf{x_0}$ (i.e., delay, filter, and sum), we see that the matched filter beamformation weights are

$$\boxed{w^M\left(\mathbf{x},f|\mathbf{x_0}\right) = -H_t^*(f)\,\frac{\exp\left(j2\pi f\,|\mathbf{x}-\mathbf{x_0}|/c_0\right)}{4\pi\,|\mathbf{x}-\mathbf{x_0}|}} \tag{5.6}$$

which can be described operationally as follows:

- To each signal acquired at location $\mathbf{x}$ introduce a time advance equal to $|\mathbf{x}-\mathbf{x_0}|/c_0$ and an amplitude weight equal to $1/\left(4\pi|\mathbf{x}-\mathbf{x_0}|\right)$.
- Sum all such time-advanced and weighted signals.
- Temporally filter the resulting sum with $h_t^*(-t)$, i.e., the filter matched to $h_t(t)$.
- Sample at *t=0*.

Reception Beamformation as Backpropagation[12]

Let us now suppose that our sensing aperture is planar, and is in the plane at *z=0,* so the sensed signal is $\phi(x,y,0,t) \underset{x,y,t}{\Leftrightarrow} \Phi_z(u,v,0,f)$. An alternative approach to imaging the point source at x_0, y_0, z_0 is to backpropagate the received signal to the plane at $z = z_0$ and to evaluate the result at x_0, y_0. We take the point source to be in positive half space, so the sensed wavefield is propagating towards negative *z* and we only have to be concerned with non-negative *z*.

Because we want to cast backpropagation as a filtering operation, the output of which is ultimately sampled at a point in time (chosen arbitrarily to be *t=0*), we introduce a backpropagation filter $a_f^B(x,y,z,f)$ such that

$$\begin{aligned}\left[\phi(x,y,0,t) \underset{x,y,t}{*} a^B(x,y,z,t)\right]_{\mathbf{x_0},0} &= \int df\left[\phi_f(x,y,0,f) \underset{x,y}{*} a_f^B(x,y,z,f)\right]_{\mathbf{x_0}} \\ &= \int df\left[\Im_{u,v}^{-1}\left\{\Phi_z(u,v,0,f)\,A_f^B(u,v,z,f)\right\}\right]_{\mathbf{x_0}}\end{aligned} \tag{5.7}$$

By inspection we can associate $A_f^B(x,y,z,f)$ with the backpropagation operator of eq. (4.29). For generality we also introduce a reception filter $H_r(f)$. Thus

$$
\begin{aligned}
a_f^B(x,y,z,f) &= H_r(f)\,\Im_{u,v}^{-1}\left\{\exp\left(j2\pi\frac{f}{c_0}z\sqrt{1-\left(\frac{\hat{s}c_0}{f}\right)^2}\right)\right\} \\
&= H_r(f)\,2\,\Im_{u,v}^{-1}\left\{\frac{\partial}{\partial z}G_z^*(\hat{s},z,f)\right\} \\
&= H_r(f)\,2\frac{\partial}{\partial z}\left[g_f^*(-x,-y,z,f)\right] \\
&= H_r(f)\,2z\left[j2\pi\frac{f}{c_0}\sqrt{x^2+y^2+z^2}-1\right]\frac{\exp\left(j2\pi\frac{f}{c_0}\sqrt{x^2+y^2+z^2}\right)}{4\pi\left(x^2+y^2+z^2\right)^{3/2}}
\end{aligned}
\tag{5.8}
$$

Note that this filter, as defined, operates in the propagation regime; in the evanescent regime where $\hat{s} > f/c_0$, it serves to further attenuate the signal. The backpropagation filter can thus be written

$$
\boxed{a_f^B(\mathbf{x},f) = H_r(f)\,\frac{2z}{|\mathbf{x}|}\left[\frac{1-j2\pi f|\mathbf{x}|/c_0}{|\mathbf{x}|}\right]\frac{\exp\left(j2\pi f|\mathbf{x}|/c_0\right)}{4\pi|\mathbf{x}|}}
\tag{5.9}
$$

where $|\mathbf{x}| = \sqrt{x^2+y^2+z^2}$. Substituting this in the convolution integral of eq. (5.7) and interpreting it as a beamforming integral, we see the backpropagation beamformation weights are

$$
\boxed{w^B\left(\mathbf{x},f|\mathbf{x_0}\right) = H_r(f)\,\frac{2z_0}{|\mathbf{x}-\mathbf{x_0}|}\left[\frac{1-j2\pi f|\mathbf{x}-\mathbf{x_0}|/c_0}{|\mathbf{x}-\mathbf{x_0}|}\right]\frac{\exp\left(j2\pi f\,|\mathbf{x}-\mathbf{x_0}|/c_0\right)}{4\pi\,|\mathbf{x}-\mathbf{x_0}|}}
$$

which can be described operationally as:

- To each signal acquired at location $\mathbf{x}$ introduce a time advance equal to $|\mathbf{x}-\mathbf{x_0}|/c_0$, an amplitude weight equal to $z_0/2\pi|\mathbf{x}-\mathbf{x_0}|^3$, and a filter with a frequency response of $H_r(f)\left(1-j2\pi f|\mathbf{x}-\mathbf{x_0}|/c_0\right)$.
- Sum all such time-advanced, weighted, and filtered signals.
- Sample at *t=0*.

This is essentially, for most situations of interest, the matched filter case with $H_t^*(f)$ replaced by the combination of a differentiating filter $j2\pi f$ and a reception filter $H_r(f)$. The backpropagation approach offers no guidance as to the desirable characteristics of the reception filter.

Reception Beamformation as Inverse Filtering

Let our sensing aperture once again be planar in the plane at *z=0*. A third approach to imaging the point source at x_0, y_0, z_0 is to use an inverse filter to reverse the effects of propagation. We again take the point source to be in positive half space. Our sensed signal is $\phi(x,y,0,t) \underset{x,y,t}{\Leftrightarrow} \Phi_z(u,v,0,f)$ where

$$\phi(x,y,z,t) = \left[h_t(t)\ {}^3\delta(x-x_0, y-y_0, z-z_0)\right] \underset{x,y,z,t}{*} g(x,y,z,t) \tag{5.10}$$

from which follows, taking the marginal Fourier transform with respect to time and the two spatial coordinates *x* and *y*

$$\begin{aligned}\Phi_z(u,v,0,f) &= H_t(f)\, G_z(u,v,z_0,f) \exp\left(-j2\pi\left[ux_0 + vy_0\right]\right) \\ &= H_t(f) \frac{j \exp\left\{-j2\pi \frac{f}{c_0}|z_0| \sqrt{1-\left(\frac{\hat{s}c_0}{f}\right)^2}\right\}}{4\pi \frac{f}{c_0} \sqrt{1-\left(\frac{\hat{s}c_0}{f}\right)^2}} \exp\left(-j2\pi\left[ux_0 + vy_0\right]\right)\end{aligned} \tag{5.11}$$

(We subsequently ignore the distinction between $|z_0|$ and z_0 because of the positive half space constraint.) Let us first introduce a temporal reception filter $H_r(f)$ that operates across the aperture; we thus replace $H_t(f)$ with $H_r(f)H_t(f) = H_{rt}(f)$.

Note that eq. (5.11) is phase linear in z, which suggests a Fourier transform if we identify the correct change of variables. We do this as follows.

$$\begin{aligned}\int df\ \Phi_z(u,v,0,f)\, H_r(f) \frac{4\pi}{j} \frac{f}{c_0} \sqrt{1-\left(\frac{\hat{s}c_0}{f}\right)^2}\ \delta\left(f - c_0 s \cdot \mathrm{sgn}\{w\}\right) \\ = H_{rt}\left(c_0 s \cdot \mathrm{sgn}\{w\}\right) \exp\left(-j2\pi\left[ux_0 + vy_0 + wz_0\right]\right)\end{aligned} \tag{5.12}$$

Here, *s* is the radial frequency variable in spherical coordinates, such that $s^2 = u^2 + v^2 + w^2 = \hat{s}^2 + w^2$. Eq. (5.12) can be verified by direct substitution, taking care with the signs of *f* and *w*. It is remarkable in that the right side of the equation (in the limit as $H_{rt}(f)$ is broadband and zero phase) is the three dimensional Fourier transform of ${}^3\delta(x-x_0, y-y_0, z-z_0)$, which is our original source.

To identify the associated inversion filter, we take the inverse marginal Fourier transform of the left side of eq. (5.12).

$$\Im^{-1}_{u,v,w}\left\{\int df\ \Phi_z(u,v,0,f)\,H_r(f)\,\frac{4\pi}{j}\frac{f}{c_0}\sqrt{1-\left(\frac{\hat{s}c_0}{f}\right)^2}\ \delta\left(f-c_0 s\cdot\mathrm{sgn}\{w\}\right)\right\}$$
$$=\int df\ \phi_f(x,y,0,f)\underset{x,y}{*}\Im^{-1}_{u,v,w}\left\{H_r(f)\,\frac{4\pi}{j}\frac{f}{c_0}\sqrt{1-\left(\frac{\hat{s}c_0}{f}\right)^2}\ \delta\left(f-c_0 s\cdot\mathrm{sgn}\{w\}\right)\right\} \tag{5.13}$$

The inversion filter is thus

$$a^I_f(\mathbf{x},f)=\Im^{-1}_{u,v,w}\left\{H_r(f)\,\frac{4\pi}{j}\frac{f}{c_0}\sqrt{1-\left(\frac{\hat{s}c_0}{f}\right)^2}\ \delta\left(f-c_0 s\cdot\mathrm{sgn}\{w\}\right)\right\} \tag{5.14}$$

Taking the inverse Fourier transform with respect to *w*, using the sifting properties of the Dirac delta

$$a^I_f(\mathbf{x},f)=\Im^{-1}_{u,v}\left\{H_r(f)\,\frac{4\pi}{j}\frac{f}{c_0^2}\exp\left(j2\pi\frac{f}{c_0}z\sqrt{1-\left(\frac{\hat{s}c_0}{f}\right)^2}\right)\right\} \tag{5.15}$$

But this is just the backpropagation filter multiplied by some new temporal frequency terms. Using eq. (5.9)

$$\boxed{a^I_f(\mathbf{x},f)=-H_r(f)\,\frac{4z}{|\mathbf{x}|}\left[\frac{j2\pi f}{c_0^2}\right]\left[\frac{1-j2\pi f|\mathbf{x}|/c_0}{|\mathbf{x}|}\right]\frac{\exp\left(j2\pi f|\mathbf{x}|/c_0\right)}{4\pi|\mathbf{x}|}} \tag{5.16}$$

The inversion beamformation weights are thus

$$\boxed{w^I\left(\mathbf{x},f|\mathbf{x_0}\right)=-H_r(f)\,\frac{4z_0}{|\mathbf{x}-\mathbf{x_0}|}\left[\frac{j2\pi f}{c_0^2}\right]\left[\frac{1-j2\pi f|\mathbf{x}-\mathbf{x_0}|/c_0}{|\mathbf{x}-\mathbf{x_0}|}\right]\frac{\exp\left(j2\pi f\,|\mathbf{x}-\mathbf{x_0}|/c_0\right)}{4\pi\,|\mathbf{x}-\mathbf{x_0}|}} \tag{5.17}$$

Operationally this is:

- To each signal acquired at location $\mathbf{x}$ introduce a time advance equal to $|\mathbf{x}-\mathbf{x_0}|/c_0$, an amplitude weight equal to $z_0/\pi c_0^2|\mathbf{x}-\mathbf{x_0}|^3$, and a filter with a frequency response of $H_r(f)\left(j2\pi f\right)\left(1-j2\pi f|\mathbf{x}-\mathbf{x_0}|/c_0\right)$.
- Sum all such time-advanced, weighted, and filtered signals.
- Sample at *t=0*.

Inversion beamformation is essentially the same as backpropagation beamformation with the addition of a second differentiating filter $j2\pi f$. The reception filter $H_r(f)$ should be chosen to make the total response $H_{rt}(f)$ broadband and zero phase.

Summary

These three formulations, cast as filtering problems and reduced to beamformation weights, are summarized below.

Matched Filter
$$\int df\ \phi_f(x,y,z,f) \underset{x,y,z}{*} a_f^M(x,y,z,f)$$
$$a_f^M(\mathbf{x},f) = -H_t^*(f)\,\frac{\exp\left(j2\pi f\,|\mathbf{x}|/c_0\right)}{4\pi|\mathbf{x}|}$$
$$w^M\left(\mathbf{x},f\middle|\mathbf{x_0}\right) = -H_t^*(f)\,\frac{\exp\left(j2\pi f\,\left|\mathbf{x}-\mathbf{x_0}\right|/c_0\right)}{4\pi\,\left|\mathbf{x}-\mathbf{x_0}\right|}$$

Backpropagation Filter
$$\int df\ \phi_f(x,y,0,f) \underset{x,y}{*} a_f^B(x,y,z,f)$$
$$a_f^B(\mathbf{x},f) = H_r(f)\,\frac{2z}{|\mathbf{x}|}\left[\frac{1-j2\pi f\,|\mathbf{x}|/c_0}{|\mathbf{x}|}\right]\frac{\exp\left(j2\pi f\,|\mathbf{x}|/c_0\right)}{4\pi|\mathbf{x}|}$$
$$w^B\left(\mathbf{x},f\middle|\mathbf{x_0}\right) = H_r(f)\,\frac{2z_0}{\left|\mathbf{x}-\mathbf{x_0}\right|}\left[\frac{1-j2\pi f\left|\mathbf{x}-\mathbf{x_0}\right|/c_0}{\left|\mathbf{x}-\mathbf{x_0}\right|}\right]\frac{\exp\left(j2\pi f\,\left|\mathbf{x}-\mathbf{x_0}\right|/c_0\right)}{4\pi\,\left|\mathbf{x}-\mathbf{x_0}\right|}$$

Inversion Filter
$$\int df\ \phi_f(x,y,0,f) \underset{x,y}{*} a_f^I(x,y,z,f)$$
$$a_f^I(\mathbf{x},f) = -H_r(f)\,\frac{4z}{|\mathbf{x}|}\left[\frac{j2\pi f}{c_0^2}\right]\left[\frac{1-j2\pi f\,|\mathbf{x}|/c_0}{|\mathbf{x}|}\right]\frac{\exp\left(j2\pi f\,|\mathbf{x}|/c_0\right)}{4\pi|\mathbf{x}|}$$
$$w^I\left(\mathbf{x},f\middle|\mathbf{x_0}\right) = -H_r(f)\,\frac{4z_0}{\left|\mathbf{x}-\mathbf{x_0}\right|}\left[\frac{j2\pi f}{c_0^2}\right]\left[\frac{1-j2\pi f\left|\mathbf{x}-\mathbf{x_0}\right|/c_0}{\left|\mathbf{x}-\mathbf{x_0}\right|}\right]\frac{\exp\left(j2\pi f\,\left|\mathbf{x}-\mathbf{x_0}\right|/c_0\right)}{4\pi\,\left|\mathbf{x}-\mathbf{x_0}\right|}$$

These approaches are all motivated by the Fourier relationships of propagation and LSI filtering, rather than geometrical arguments. The latter two use planar reception apertures. Even though we solved three different problems to get three different beamformation weights, the three results have features in common.

- They all introduce identical compensating delays (i.e. focusing).
- They all introduce similar amplitude weighting (i.e., apodization).

In addition, the latter two introduce filtering, in the form of temporal derivatives, that is weakly aperture-dependent.

All three techniques work in the propagation regime, and, by design, cut off sharply in the evanescent regime. As a consequence, there are effectively no spatial frequencies preserved above f/c_0. This is not so much a matter of choice as it is a physical limit dictated by the characteristics of propagation.

We have ignored rudimentary practical issues, such as finite aperture effects, temporal bandwidth, and the like. As a consequence, we've not yet developed guidance for sidelobe control, range resolution, and so on. That comes next.

Beamformation and the Point Spread Function

The Three Dimensional Point Spread Function

Consider an acoustic imaging system with a planar aperture with which we want to image the point $\mathbf{x_0} = x_0, y_0, z_0$. Recall the pulse-echo equation (4.34), rewritten here using vector notation

$$R(f) = H_{rt}(f) \int d\mathbf{x}\, o_f(\mathbf{x}, f) \left[w_r(\mathbf{x}, f) \underset{x,y}{*} g_f(\mathbf{x}, f) \right] \left[w_t(\mathbf{x}, f) \underset{x,y}{*} g_f(\mathbf{x}, f) \right] \tag{6.1}$$

To set up the one-way imaging equation, we restrict candidate weighting functions for reception to the form

$$w_r(\mathbf{x}, f) = a_r(\mathbf{x} - \mathbf{x_0}, f) \exp\left(j2\pi f \left| \mathbf{x} - \mathbf{x_0} \right| / c_0 \right) \tag{6.2}$$

Note that all three of the beamformation weights developed in the prior section are of this form. This expresses the idealized requirement that shifting our point of focus merely shifts our aperture weighting function. Three points are important.

- This is a requirement for a shift-invariant imaging system.
- This requirement cannot be met in general with a finite-aperture system, as aperture end effects will ultimately come into play. With care, however, this requirement can be substantially met over localized regions of the field of view.
- This is the basis for dynamic focusing and scanning.

In order to characterize the one-way beamformation performance, we use an omnidirectional illumination function, i.e., a point source transmitter at the origin. The transmission aperture thus becomes a sampled version of eq. (6.2).

$$\begin{aligned} w_t(\mathbf{x}, f) &= {}^2\delta(x, y)\, a_t(\mathbf{x} - \mathbf{x_0}, f) \exp\left(j2\pi f \left| \mathbf{x} - \mathbf{x_0} \right| / c_0 \right) \\ &= {}^2\delta(x, y)\, a_t(-\mathbf{x_0}, f) \exp\left(j2\pi f \left| \mathbf{x_0} \right| / c_0 \right) \end{aligned} \tag{6.3}$$

We subsequently ignore the transmission weight $a_t(-\mathbf{x_0})$, as it can be incorporated in the transmission pulse $H_t(f)$. Following our development of the prior section, we integrate out temporal frequency to obtain the desired point of our image.

$$i(\mathbf{x_0}) = \int df\ H_{rt}(f) \int d\mathbf{x}\ o_f(\mathbf{x}, f) \left[a_r(\mathbf{x} - \mathbf{x_0}, f) \exp\left(j2\pi f |\mathbf{x} - \mathbf{x_0}|/c_0\right) \underset{x,y}{*} \frac{\exp(-j2\pi f |\mathbf{x}|/c_0)}{4\pi|\mathbf{x}|} \right] \left[\exp\left(j2\pi f |\mathbf{x_0}|/c_0\right) \frac{\exp(-j2\pi f |\mathbf{x}|/c_0)}{4\pi|\mathbf{x}|} \right] \tag{6.4}$$

For simplicity of expression this can be cast as a convolution.

$$i(\mathbf{x_0}) = \int df\ H_{rt}(f) \int d\mathbf{x}\ o_f(\mathbf{x}, f)\ s_f(\mathbf{x_0} - \mathbf{x}, f) \tag{6.5}$$

The impulse response of the imaging system is thus

$$p(\mathbf{x}) = \int df\ H_{rt}(f)\ s_f(\mathbf{x}, f) \tag{6.6}$$

where the convolution kernel is given by

$$s_f(\mathbf{x_0} - \mathbf{x}, f) = \left[a_r(\mathbf{x} - \mathbf{x_0}, f) \exp\left(j2\pi f |\mathbf{x} - \mathbf{x_0}|/c_0\right) \underset{x,y}{*} \frac{\exp(-j2\pi f |\mathbf{x}|/c_0)}{4\pi|\mathbf{x}|} \right] \left[\exp\left(j2\pi f |\mathbf{x_0}|/c_0\right) \frac{\exp(-j2\pi f |\mathbf{x}|/c_0)}{4\pi|\mathbf{x}|} \right] \tag{6.7}$$

The one-way impulse response of the imaging system focused at $\mathbf{x_0}$ can thus be expressed as

$$\boxed{p(\delta | \mathbf{x_0}) = \int df\ H_{rt}(f) \int d\mathbf{x}\ a_r(\mathbf{x}, f | \mathbf{x_0}) \frac{\exp\left(j2\pi f \left[|\mathbf{x} - \mathbf{x_0}| - |\mathbf{x} - (\mathbf{x_0} - \delta)| + |\mathbf{x_0}| - |\mathbf{x_0} - \delta|\right]/c_0\right)}{(4\pi)^2 |\mathbf{x} - (\mathbf{x_0} - \delta)|\, |\mathbf{x_0} - \delta|}} \tag{6.8}$$

This function is usually referred to as the *point spread function* of the system, in the tradition of optics. Its Fourier transform is the *transfer function* of the system.

The distance terms in eq. (4.29) have very simple geometrical interpretations.

- $|\mathbf{x} - \mathbf{x_0}|$ The distance from aperture point $\mathbf{x}$ to focal point $\mathbf{x_0}$
- $|\mathbf{x} - (\mathbf{x_0} - \delta)|$ The distance from aperture point $\mathbf{x}$ to field point $\mathbf{x_0} - \delta$
- $|\mathbf{x_0}|$ The distance from the origin to focal point $\mathbf{x_0}$
- $|\mathbf{x_0} - \delta|$ The distance from the origin to field point $\mathbf{x_0} - \delta$

A Local Expansion of the Two Dimensional Point Spread Function

Because the point spread function in a well designed imaging system is compact, we will expand eq. (6.8) assuming δ is small. For simplicity, we will consider just two dimensions, range and azimuth. The geometry is shown below.

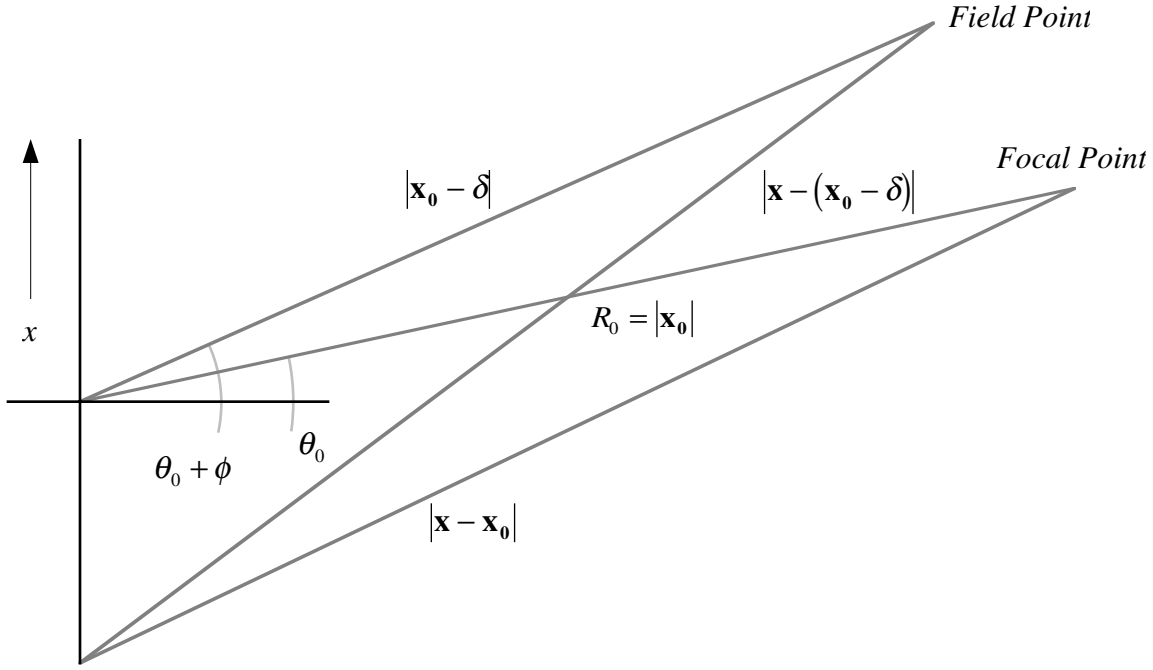

(6.9)

In polar coordinates, we locate the focal point at R_0, θ_0 (where, obviously, $R_0 = |\mathbf{x_0}|$) and the field point at $R_0 + r, \theta_0 + \phi$, where we will be interested in small r and ϕ. The associated arc length is $u = R_0\phi = |\mathbf{x_0}|\phi$ as can be seen in the figure below, and we will use *r* and *u* as our incremental parameters for the expansion.

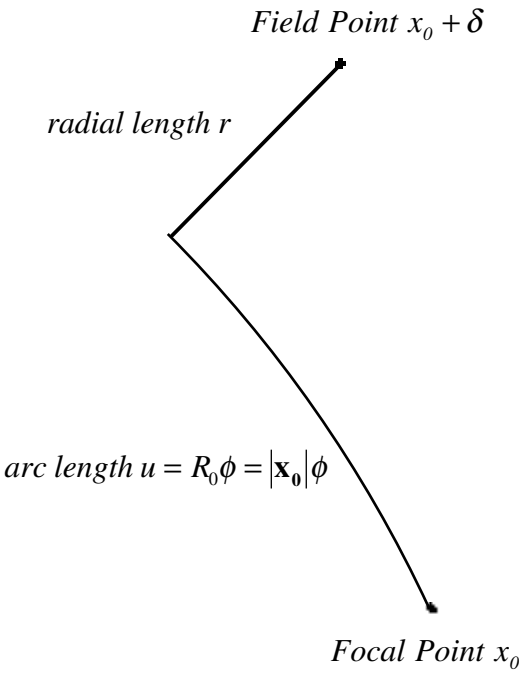

(6.10)

We expand the exponent of eq. (6.8) in a two-dimensional Taylor's series around x_0 and keep the lowest order terms; the denominator is similarly expanded. This yields

$$p(r,u) \cong \int df\ H_{rt}(f) \int dx\ \frac{a_r(x,f)}{(4\pi)^2\,|\mathbf{x}-\mathbf{x_0}|\,|\mathbf{x_0}|} \exp\left(j2\pi \left[\frac{|\mathbf{x}-\mathbf{x_0}| + |\mathbf{x_0}| - x\sin\theta_0}{|\mathbf{x}-\mathbf{x_0}|} \right] \frac{f}{c_0} r \right) \exp\left(j2\pi \left[-\frac{x\cos\theta_0}{|\mathbf{x}-\mathbf{x_0}|} \right] \frac{f}{c_0} u \right) \tag{6.11}$$

This can be simplified with the following construction.

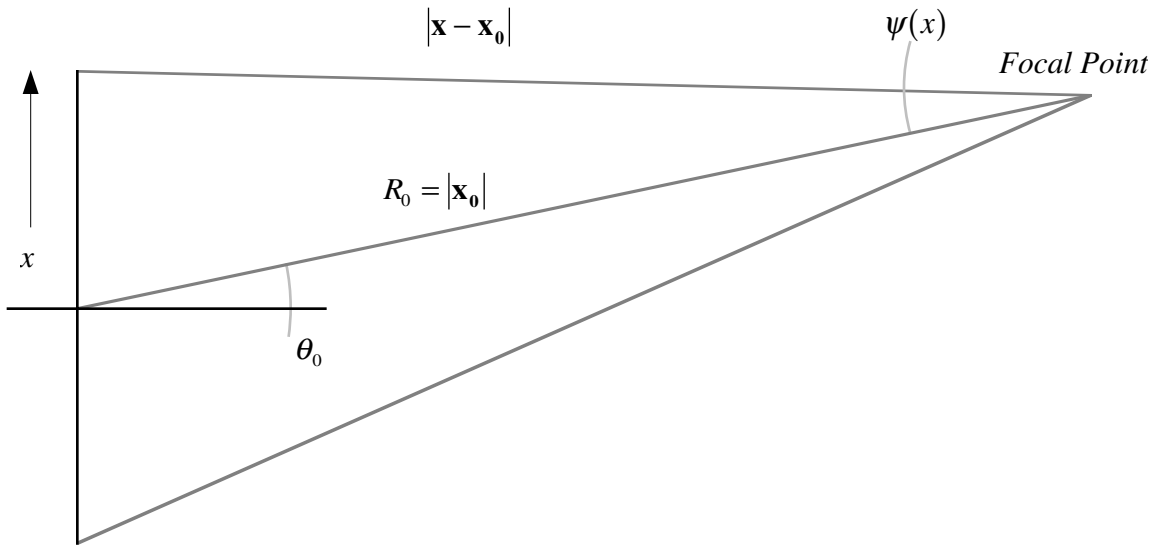

(6.12)

We define the angle $\psi(x)$ as the observation angle; it is the angle seen at the focal point between the origin and the point x on the aperture. As usual, counterclockwise rotation corresponds to increasing angle. It is readily shown using the law of sines that

$$-\frac{x\cos\theta_0}{|\mathbf{x}-\mathbf{x_0}|} = \sin\psi(x) \tag{6.13}$$

and, using the law of cosines

$$\frac{|\mathbf{x_0}| - x\sin\theta_0}{|\mathbf{x}-\mathbf{x_0}|} = \cos\psi(x) \tag{6.14}$$

Hence, substituting into eq. (6.11)

$$p(r,u) \cong \frac{1}{(4\pi R_0)^2}\int df \int dx \;\; \frac{\cos(\psi(x)+\theta_0)}{\cos\theta_0} H_{rt}(f)\, a_r(x,f) \exp\left(j2\pi[1+\cos\psi(x)]\frac{f}{c_0} r \right) \exp\left(j2\pi \sin\psi(x)\frac{f}{c_0} u \right) \tag{6.15}$$

As the aperture is finite in extent, we can associate some full observation angle and denote it Ψ; by construction, the origin can be chosen such that it bisects the full observation angle. In this way the full observation angle is bound by $\Psi < \pi$ and the angle to any aperture point by $|\psi(x)| < \pi/2$. We shall see that the azimuthal resolution of this system is ultimately limited by Ψ.

We see that eq. (6.15) can be written as a two dimensional Fourier transform with the following change of variables.

$$\begin{aligned}\rho &= \frac{f}{c_0}\left[1+\cos\psi(x)\right] \\ \upsilon &= \frac{f}{c_0}\sin\psi(x)\end{aligned} \tag{6.16}$$

By construction, there is a one-to-one correspondence between ρ,υ space and f,x space, and a coordinate transformation may be performed. The resulting Fourier integral from eq. (6.15) is

$$p(r,u) = \int d\rho \int d\upsilon\; P(\rho,\upsilon)\exp\left(j2\pi\left[\rho r + \upsilon u\right]\right) \tag{6.17}$$

We refer to $P(\rho,\upsilon)$ as the transfer function of the imaging system under consideration, as it is the Fourier transform of the impulse response. The interested reader may wish to expand $P(\rho,\upsilon)$ in terms of $H_{rt}(f)$ and $a_r(x,f)$. We will confine our investigation here to the geometry of this coordinate transformation with the goal of obtaining some insights into point spread functions.

First note that

$$\begin{aligned}\upsilon &= \rho\left[\frac{\sin\psi(x)}{1+\cos\psi(x)}\right] \\ &= \rho\tan\left(\frac{\psi(x)}{2}\right)\end{aligned} \tag{6.18}$$

We infer from this the following.

- Lines of constant location x (on the aperture) in f,x space map to diagonal lines in ρ,υ space, passing through the origin at an angle of $\psi(x)/2$ with the ρ axis.

Second, it is easily shown that

$$\left(\rho-\frac{f}{c_0}\right)^2 + \upsilon^2 = \left(\frac{f}{c_0}\right)^2 \tag{6.19}$$

from which we infer

- Lines of constant frequency f in f,x space map to circles in ρ,υ space, centered at $(\rho,\upsilon) = \left(\frac{f}{c_0},0\right)$ with radii of f/c_0.

To visualize this, consider an imaging system for which the product $H_{rt}(f)\,a_r(x,f)$ has a bounded region of support (i.e., finite aperture and bandwidth) in f,x space as shown below.

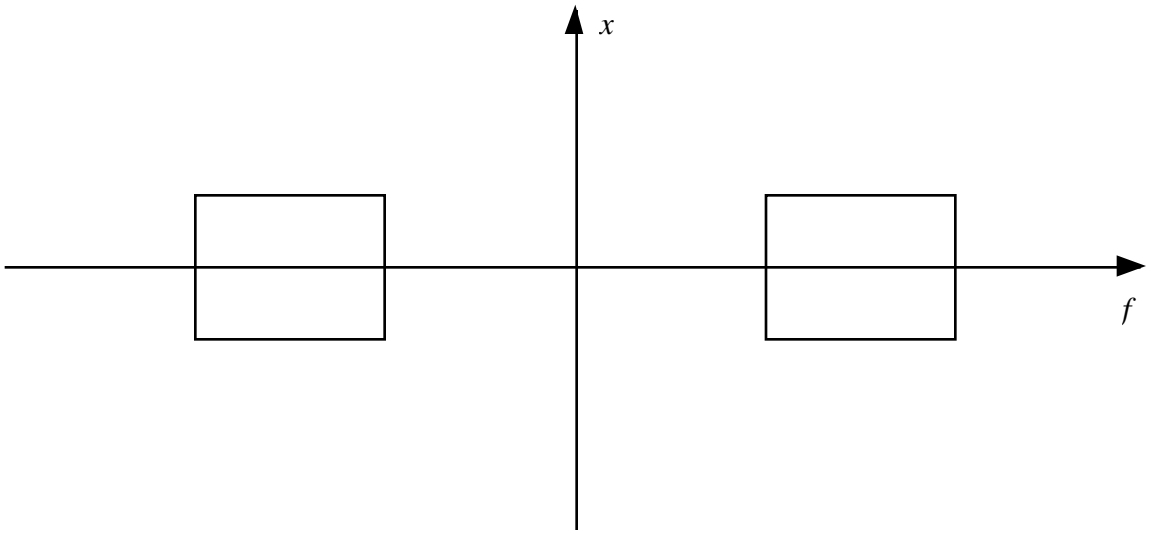

(6.20)

After the coordinate transformation, the transfer function $P(\rho,\upsilon)$ also has a finite region of support, but of a different geometry.

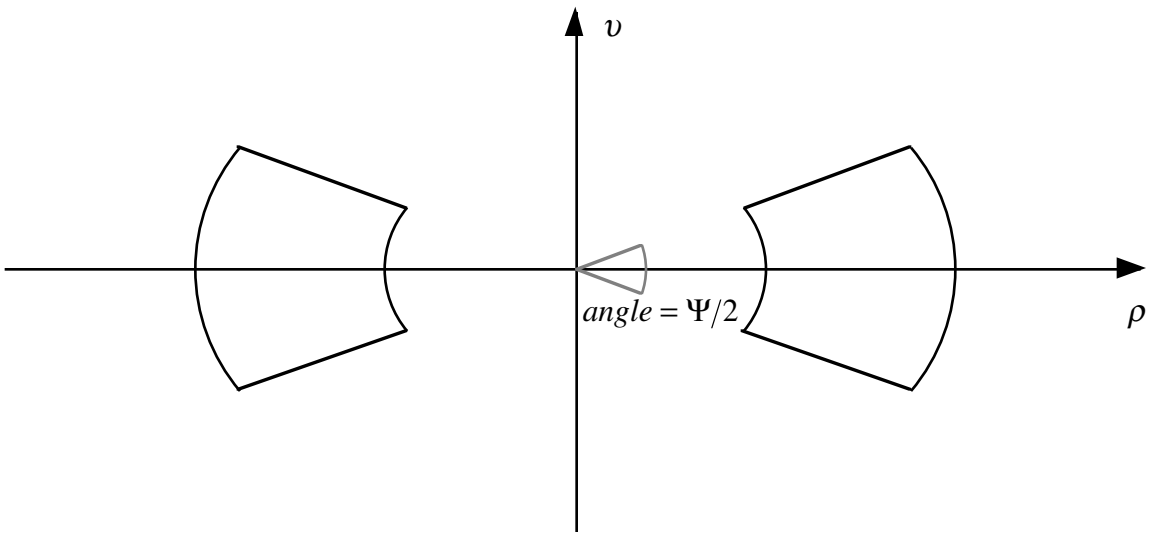

(6.21)

There are two obvious consequences.

- The effects of frequency weighting and amplitude weighting are not orthogonal.
- In the limit of infinite bandwidth and aperture, the ρ,υ plane is only half filled (as Ψ is limited to π), implying a natural limit to one-way resolution.

Let's examine the azimuthal resolution of this system for a broadside, narrowband excitation. Set

$$\begin{aligned} H_{rt}(f)\, a_r(x,f) &= \delta(f - f_0) \\ \theta_0 &= 0 \end{aligned} \tag{6.22}$$

We also want to evaluate the azimuthal resolution only, so we set $r = 0$. The full observation angle is Ψ, which corresponds to the range of integration from some $x_{\min}$ to $x_{\max}$. In this case, eq. (6.15) simplifies to

$$\begin{aligned} p(0,u) &= \frac{1}{(4\pi R_0)^2} \int_{-\infty}^{\infty} df \int_{x_{\min}}^{x_{\max}} dx \cos\psi(x)\, \delta(f - f_0) \exp\left(j2\pi \sin\psi(x) \frac{f}{c_0} u \right) \\ &= \frac{1}{(4\pi R_0)^2} \int_{x_{\min}}^{x_{\max}} dx \cos\psi(x) \exp\left(j2\pi \sin\psi(x) \frac{f_0}{c_0} u \right) \\ &= \frac{1}{(4\pi R_0)^2} \int_{\sin(-\Psi/2)}^{\sin(\Psi/2)} d\xi \exp\left(j2\pi \xi \frac{u}{\lambda_0} \right) \end{aligned} \tag{6.23}$$

Here we have made the customary substitution $f_0/c_0 = 1/\lambda_0$. The integral is simply the (inverse) Fourier transform of $\text{rect}\left[\xi / 2\sin(\Psi/2)\right]$, hence

$$p(0,u) = \left[\frac{2\sin(\Psi/2)}{(4\pi R_0)^2} \right] \text{sinc}\left(\frac{2\sin(\Psi/2)}{\lambda_0} u \right) \tag{6.24}$$

The Rayleigh criterion for the azimuthal resolution of this system can be seen by inspection; as Ψ is bounded, the resolution also has an upper limit.

$$\boxed{\textit{resolution} = \frac{\lambda_0}{2\sin(\Psi/2)} < \frac{\lambda_0}{2}} \tag{6.25}$$

This limit is the Rayleigh limit for a one-way linear aperture.

In the broadside illumination case we have used here, the resolution can be expressed in terms of the f-number. By construction

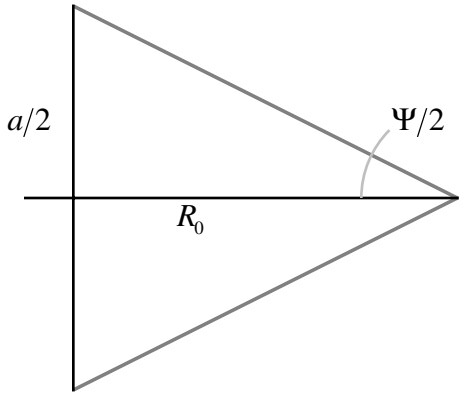

(6.26)

Using $f_{\#} = R_0/a$ we see that the resolution can be expressed as

$$\frac{\lambda_0}{2\sin(\Psi/2)} = \frac{\lambda_0}{a\Big/\sqrt{R_0^2 + (a/2)^2}} = f_{\#}\,\lambda_0\sqrt{1+\frac{1}{4f_{\#}^2}} \tag{6.27}$$

Thus our rule of thumb that azimuthal resolution equals $f_{\#}\lambda_0$ holds for f-numbers greater than about one; below that, adding more aperture is increasingly ineffectual. The graph below plots azimuthal resolution (in wavelengths) versus f-number; both eq. (6.27) and our rule of thumb are plotted.

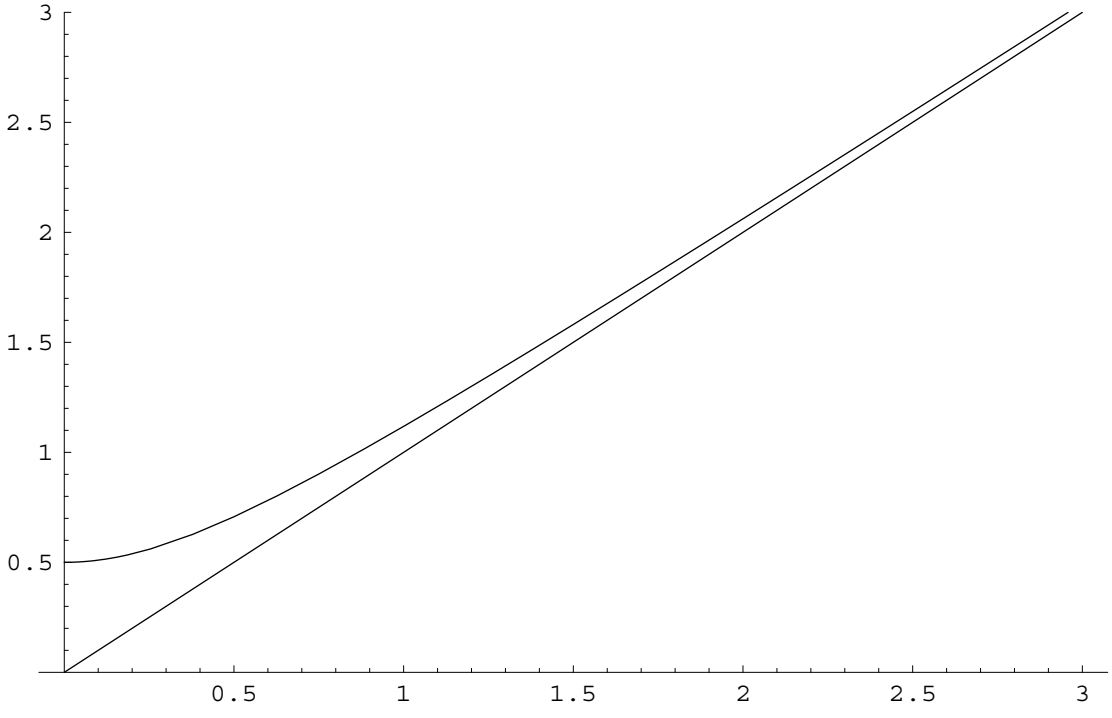

(6.28)

The Fraunhofer Expansion of the Two Dimensional Point Spread Function

The Fraunhofer expansion of the point spread function is a further approximation to the full integral expression, eq. (6.8). Its advantage is its simplicity.

The local expansion in the prior section approximated

$$p\left(\delta\middle|\mathbf{x_0}\right)=\int df\ H_{rt}(f)\int d\mathbf{x}\ a_r\left(\mathbf{x},f\middle|\mathbf{x_0}\right)\frac{\exp\left(j2\pi\, f\left[\left|\mathbf{x}-\mathbf{x_0}\right|-\left|\mathbf{x}-\left(\mathbf{x_0}-\delta\right)\right|+\left|\mathbf{x_0}\right|-\left|\mathbf{x_0}-\delta\right|\right]/c_0\right)}{(4\pi)^2\left|\mathbf{x}-\left(\mathbf{x_0}-\delta\right)\right|\left|\mathbf{x_0}-\delta\right|} \tag{6.29}$$

by expanding the exponent and the denominator separately in a two dimensional Taylor's series, in *r* and *u*. The Fraunhofer expansion approximates the integral by similarly expanding terms in a *three* dimensional Taylor's series, in *r* and *u* and *x.*

$$p(r,u)\cong\frac{1}{\left(4\pi R_0\right)^2}\int df\ \int dx\ H_{rt}(f)\,a_r(x,f)\exp\left(j2\pi\frac{2f}{c_0}r\right)\exp\left(-j2\pi\frac{x\cos\theta_0}{R_0}\frac{f}{c_0}u\right) \tag{6.30}$$

The Fourier relationship

$$p(r,u)=\int d\rho\int d\upsilon\ P(\rho,\upsilon)\exp\left(j2\pi\left[\rho r+\upsilon u\right]\right) \tag{6.31}$$

follows directly from the substitutions

$$\begin{aligned}\rho&=\frac{2f}{c_0}\\ \upsilon&=-\frac{x\cos\theta_0}{R_0}\frac{f}{c_0}\end{aligned} \tag{6.32}$$

The interested reader is invited to explore the geometry of this coordinate transformation. Even with this simplification, the effects of amplitude weighting and frequency weighting are still not orthogonal.

Orthogonality can be achieved with the narrowband Fraunhofer expansion. In this, eq. (6.32) is written assuming some center frequency f_0. This has the advantage that, when $a_r(\cdot)$ is amplitude weighting only, the resulting approximation is separable:

$$\begin{aligned}p(r,u)&\cong\frac{1}{\left(4\pi R_0\right)^2}\left[\int df\ H_{rt}(f)\exp\left(j2\pi\frac{2f}{c_0}r\right)\right]\left[\int dx\ a_r(x)\ \exp\left(-j2\pi\frac{x\cos\theta_0}{R_0}\frac{f_0}{c_0}u\right)\right]\\ &=\left[\int d\rho\ P(\rho)\exp(j2\pi\rho r)\right]\left[\int d\upsilon\ P(\upsilon)\ \exp(j2\pi\upsilon u)\right]\\ &=p(r)\,p(u)\end{aligned} \tag{6.33}$$

where we can see by inspection (neglecting scale factors, and using the standard notation for Fourier pairs $a_r(x) \Leftrightarrow A_r(u)$)

$$\begin{aligned} p(r) = h_{rt}\left(\frac{2}{c_0} r\right) \quad &\Leftrightarrow \quad P(\rho) = H_{rt}\left(\frac{c_0}{2}\rho\right) \\ p(u) = A_r\left(\frac{\cos\theta_0}{R_0\lambda_0} u\right) \quad &\Leftrightarrow \quad P(\upsilon) = a_r\left(\frac{R_0\lambda_0}{\cos\theta_0}\upsilon\right) \end{aligned} \tag{6.34}$$

This is the approximation that is used most often in rough characterization of acoustic imaging systems, and it's basically the result we saw earlier using simple geometrical arguments. It says:

- The range resolution is the imaging pulse, scaled by two for the round trip.
- The azimuthal resolution is the Fourier transform of the aperture, appropriately scaled with the obliquity factor, range, and wavelength.

One should use this approximation with care. In modern ultrasound systems, both the narrowband assumption and the small aperture (i.e., large f-number) assumption are often violated.

The Transmission/Reception Point Spread Function

Thus far we have confined ourselves to the discussion of the one-way, or reception, PSF by modeling the transmitter as a point source which provides no azimuthal resolution. In actual systems, of course, designers use transmission beamformers to focus acoustic energy.

The resulting PSFs are complex to model accurately. Using the techniques of the prior sections for two-way analysis, and assuming a narrowband Fraunhofer expansion, we can come to a rough description of the resolution characteristics of a fixed-focus transmit/dynamic-focus receive system.

- The range resolution is unchanged from our prior description, being dominated by the round-trip imaging pulse $h_{rt}(t)$.
- The azimuthal resolution is equivalent to a one-way system whose aperture is the convolution of the transmission and reception apertures.

The last point means that a system will exhibit essentially one-way azimuthal resolution away from the transmission focus, and improved two-way azimuthal resolution within the depth-of-focus of the transmission beam.

The complexity of analysis for two-way operation should not obscure a central fact: the image field is the convolution of the object field and the two-way PSF. The PSF is thus a filter through which the object is seen, and image quality depends in the most fundamental way on this filter.

Summary

Images are formed through the convolution of the object field with the system point spread function (or, equivalently, weighting the Fourier transform of the object field with the system transfer function). This is a direct consequence of: (1) the LSI character of propagation and low-level scattering; (2) our choice of LSI processing for formation of the image; and (3) the design of PSFs that are compact and relatively invariant as the system scans through a neighborhood.

The design of PSFs for ultrasound can be complex because of the interaction of range and azimuthal characteristics, and there is no substitute for simulation tools and careful empirical evaluation in a diagnostic context.

Sampling and Image Processing

Sampling Requirements in Two Dimensions

We have seen how the point spread function of an imaging system is a convolution kernel—equivalently, how its transfer function is a filter—through which the system maps an object field to an image field

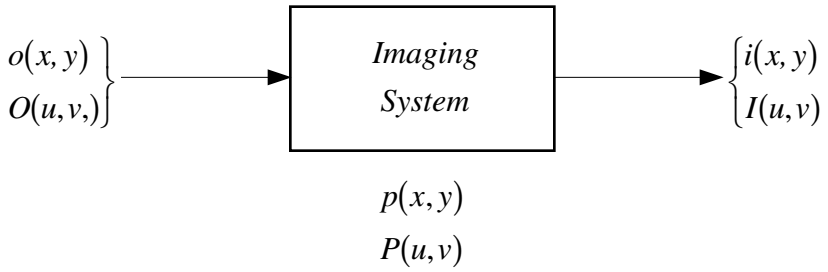

(7.1)

We need to be mindful that this model applies only in localized regions in even the best designed systems, as the PSF will vary in a gradual way over space. Within any such localized region, however, the PSF can be viewed as a filter, suppressing some spatial frequencies and passing others. When our aperture is finite (as it always is) and our imaging pulse is band-limited (which is a function of system design), the transfer function of the imaging system has a finite region of support, i.e., it is two-dimensionally band-limited, as we saw earlier. As a direct consequence, the image is likewise confined to the same region of support.

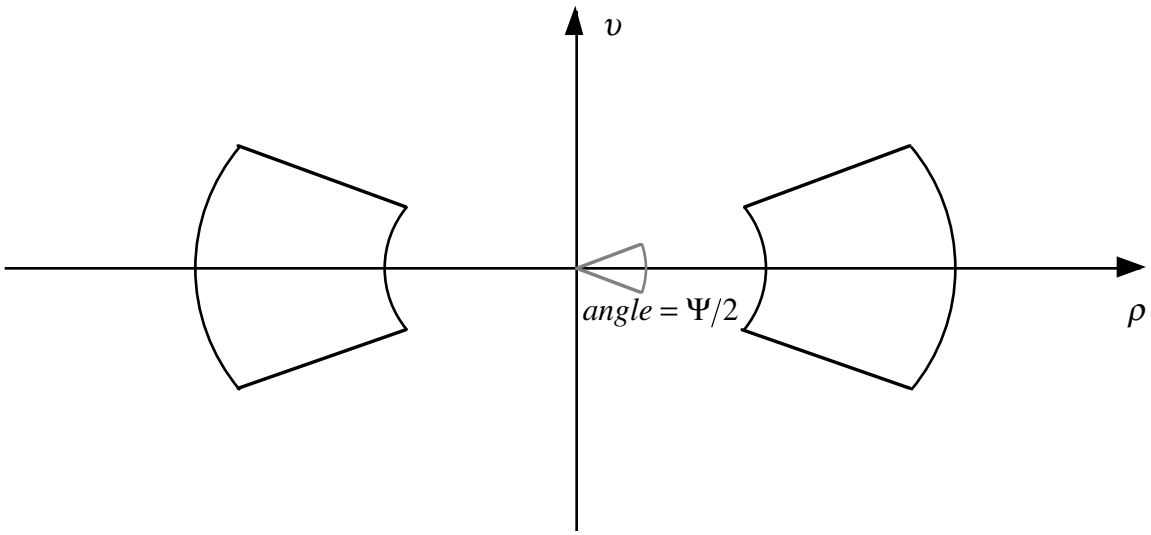

(7.2)

Because we are dealing with real signals and systems, the Fourier transform of the image field (confined to the regions shown above) will exhibit hermetian symmetry. As a consequence, only one of the regions is necessary to fully characterize the image. Using

the narrowband Fraunhofer expansion we can estimate the extent of either region; neglecting scale factors:

$$p(r) = h_{rt}\left(\frac{2}{c_0} r\right) \quad \Leftrightarrow \quad P(\rho) = H_{rt}\left(\frac{c_0}{2}\rho\right)$$
$$p(u) = A_r\left(\frac{\cos\theta_0}{R_0\lambda_0} u\right) \quad \Leftrightarrow \quad P(\upsilon) = a_r\left(\frac{R_0\lambda_0}{\cos\theta_0}\upsilon\right) \tag{7.3}$$

It is convenient to define the extent of $P(\upsilon)$ using the two way f-number, and the extent of $P(\rho)$ using the inverse full fractional bandwidth of the imaging pulse (in this context, full fractional bandwidth refers to the region of support of the imaging pulse frequency response, not the usual 3 dB bandwidth). In the figure to follow, let

$f_\# =$ System two way f - number

$$f_B = \frac{f_0}{\text{full bandwidth of imaging pulse}} = \text{Inverse full fractional bandwidth}$$

We can think of f_B as the imaging pulse analog of the f-number. Applying these limits to eq. (7.3):

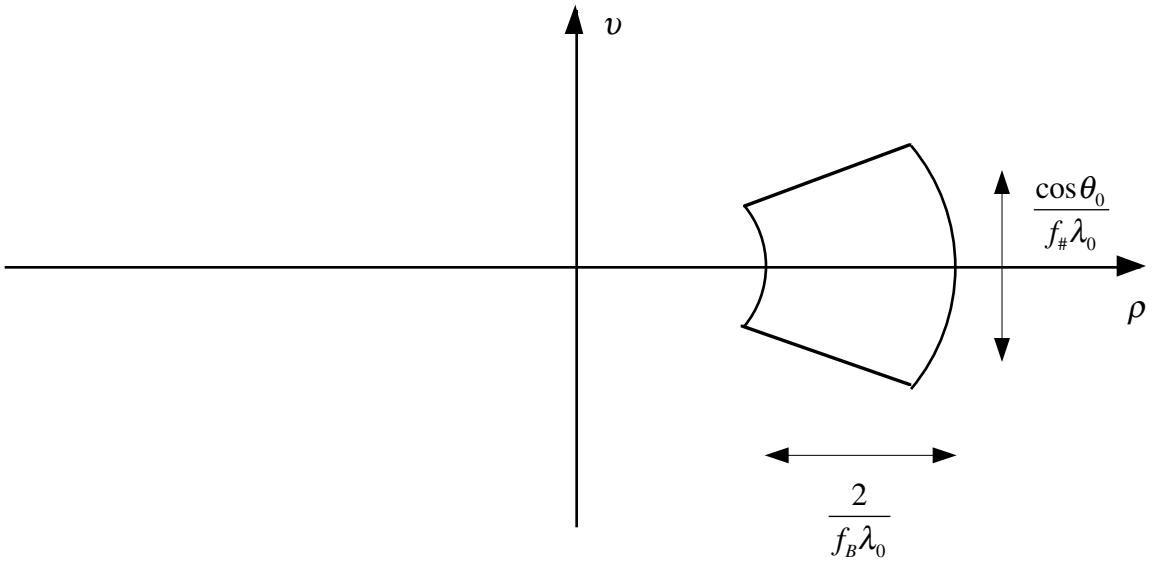

(7.4)

So far, we have considered the imaging process to be a continuous one, and of course it is not. Consider an image sampled in both range and azimuth. As is well known, adequate spatial sampling (permitting perfect reconstruction in principle) of the bandlimited signal represented above requires:

$$\text{azimuth sampling period} = \frac{f_{\#}\lambda_0}{\cos\theta_0}$$
$$\text{range sampling period} = \frac{f_B\lambda_0}{2} \tag{7.5}$$

For example, consider a system with a receive $f_{\#} = 2$ and a transmit $f_{\#} = 2$, steered straight ahead. At the transmit focus, the system has an effective two-way $f_{\#} = 1$, so the spacing for scan lines should be λ_0. (Note that the Rayleigh criterion for resolution is the same as the Nyquist criteria for sampling.) If the full fractional bandwidth is 50%, then $f_B = 2$ and the range sampling period should also be λ_0.

There are some practical points to consider.

- Any real system will not exhibit a sharp, idealized cutoff. In azimuth, any apodization applied to the transmit or receive apertures will taper the response smoothly to zero; in range, the envelope of the imaging pulse will usually be smoothly tapered as well. This means that there is latitude to adjust the sample grid to optimize the system for specific situations.
- Sampling in azimuth is almost always more expensive than sampling in range. As a consequence, compromises in sample rates are usually most egregious there.
- The two most compelling reasons to compromise sampling density (especially in azimuth) are: (1) to meet frame rate requirements, and (2) to satisfy some system limitations (such as memory limits, data rate limits, etc.).

Post-Detection Sampling Requirements

The image we have been considering thus far is the result of LSI processing. The exception to this is the sampling process (and any other process to shift the spectrum in the frequency domain), but these are reversible as long as certain criteria are met. The process of detection—necessary for the display of the image—fundamentally changes the sampling requirements of the image.

Consider a squared-magnitude detection process. (While diagnostic ultrasound generally uses log-magnitude detection, the conclusion to follow is not qualitatively affected.) As multiplication in one domain is convolution in the other, the region of support of the post-detection image spectrum is approximately four times the area of the pre-detection image spectrum.

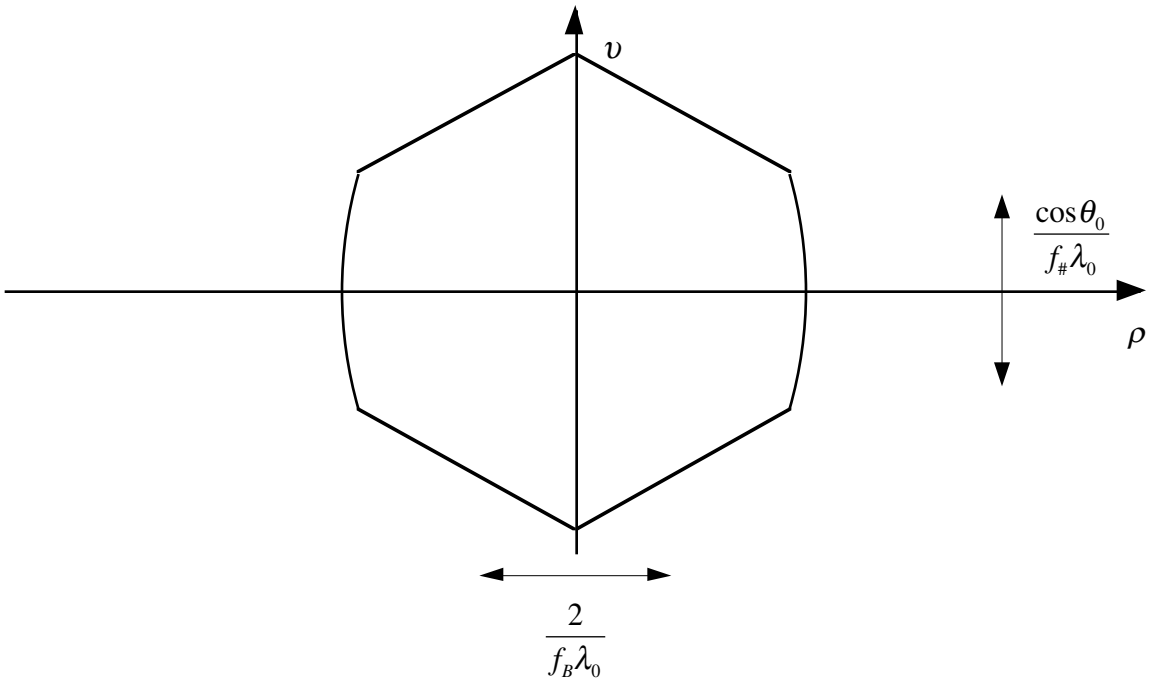

(7.6)

The conclusion is that our post-detection sampling requirements are approximately *four times*—twice in azimuth and twice in range—as our pre-detection sampling requirements[13]. These theoretical results are often violated in practical diagnostic ultrasound, with consequential corruption of image information due to aliasing.

The necessity of an adequately fine sample grid to preserve all the information in the post-detection image is easily seen using the frequency domain analysis above. Interestingly, there are theoretical grounds[14] for the position that adequate sampling of the post-detection image is sufficient to preserve all the pre-detection information also, as the detection is (almost always) reversible in principle.

Shift-Variance in Diagnostic Ultrasound

There are endless opportunities to degrade an acoustic image through the introduction of shift-variance. We have examined a key requirement for shift-invariance earlier, specifically that the PSF be substantially invariant throughout all localized regions of the image field. Most modern beamformer-based systems meet this criterion to a greater or lesser degree (although in this regard many fall short of older mechanically-scanned systems, where PSF invariance was ensured by physical constraints). We will identify here two other sources of shift-variance, which can be substantially eliminated with careful system design.

Shift Variance due to Undersampling

Historically, it has been common in diagnostic ultrasound to use a density of scan lines more or less adequate to sample an image in azimuth *prior to detection*. As a consequence ultrasound images are commonly undersampled post-detection by a factor of two.

There are two consequences of the resulting aliasing. First, the image becomes shift-variant. As is known[15], when a signal is undersampled, the resulting "reconstructed" signal will vary with the alignment of the sample grid and the original signal. In ultrasound, this is demonstrable by shifting, in azimuth, the object field relative to the grid of scan lines by distances that are small relative to the scan line spacing. A shift invariant system will exhibit no changes in the image as this translation is performed.

Second, image information is lost. When a signal is undersampled by a factor of two, the frequency spectrum is folded over in such a way that higher frequencies are overlaid on lower frequencies. This process is in general irreversible; low frequency information is corrupted and high frequency information is irretrievable.

Shift Variance due to Geometric Distortion

When an imaging system introduces systematic errors in its mapping of points in the object field to points in the image field, the visible consequence is geometric distortion. This can usually be seen, when present, by suitable translation of the sampling grid over the object field.

Geometric distortion is often associated technically with the use of multiple simultaneous beams. The promise of multi-beam technology for imaging, of course, is integer-multiple increase in temporal resolution. In conventional application, however, the deliberate misalignment of transmission and reception beams introduces an asymmetry in which the resulting "scan lines" are no longer lines, but curves—indeed, it becomes difficult to satisfactorily define what loci they follow.

Pre-Detection Image Processing

Manipulation of the image prior to detection is theoretically attractive, as the system designer can synthesize a class of signals, or samples, as an alternative to acquiring them directly from the aperture. This can be used to increase performance and to reduce costs.

The linearity of the acquisition process can be extended to image processing, with the advantage of predictable system performance. For example, if we average two samples of the pre-detected image, we can think of the resulting third sample in three different ways:

- as an output sample of a filter on the underlying band-limited image.
- as an image sample that would have been acquired by the average of the two point spread functions associated with the two original samples.
- as an image sample that would have been acquired by the average of the two apertures associated with the two original samples.

It is important to remember that these perspectives are incorrect when applied to similar operations post-detection, for the detection process breaks the chain of linear operations used to form the image to this point.

The specific applications for pre-detection image processing in diagnostic ultrasound are manifold. Some interesting ones include the following.

- Reconstruction, or partial reconstruction, of the image prior to detection[16]. In an otherwise properly sampled image, this technique can eliminate post-detection undersampling as a source of shift-variance and information loss without increasing the time to acquire the image.
- Elimination of geometric distortion in multi-beam operation[16]. The asymmetry introduced by multiple beams can be removed by careful filtering of the resulting pre-detection image, thus permitting substantially higher temporal resolution.
- Synthetic aperture. Large, high resolution apertures can be synthesized from smaller ones.
- Deconvolution of the image to increase the transmit depth of focus[17]. In this technique, the quadratic phase error associated with the transmission aperture can be partially corrected.

As the hardware for real-time image processing becomes ever more cost-effective, we expect growing practical interest and innovation in pre-detection image processing.

---

[1] Ronald N. Bracewell, "The Fourier Transform and its Applications," Second Edition, McGraw-Hill, 1978

[2] Athanasios Papoulis, "The Fourier Integral and its Applications," McGraw-Hill, 1962

[3] Norbert Wiener, "The Fourier Integral and Certain of its Applications," Dover, 1958; originally Cambridge University Press, 1933

[4] Ronald N. Bracewell, "Two-Dimensional Imaging," Prentice-Hall, 1995

[5] Athanasios Papoulis, "Systems and Transforms with Applications in Optics," McGraw-Hill, 1968

[6] Eugen Skudrzyk, "The Foundations of Acoustics," Springer-Verlag, 1971. See especially section 2.8, "Basic Theory of Internal Friction," and section 13.12, "The Effect of Viscocity."

[7] Joseph W. Goodman, "Introduction to Fourier Optics," McGraw-Hill, 1968

[8] Philip M. Morse and K. Uno Ingard, "Theoretical Acoustics," Princeton University Press, 1968. See especially chapter 8, "The Scattering of Sound."

[9] P. Stepanishen, M. Forbes and S. Letcher, "The Relationship between the Impulse Response and Angular Spectrum Methods to Evaluate Acoustic Transient Fields," J. Acoust. Soc. Am., vol. 90, no. 5, Nov. 1991

[10] A. R. Selfridge, G. S. Kino and B. T. Khuri-Yakub, "A Theory for the Radiation Pattern of a Narrow-Strip Acoustic Transducer," Appl. Phys. Lett., vol. 37, no. 1, Jul. 1980

[11] Robert C. Waag et. al., "Cross-Sectional Measurements and Extrapolation of Ultrasonic Fields," IEEE Trans. Sonics and Ultrasonics, vol. SU-32, no. 1, Jan. 1985

[12] Dong-Lai Liu and Robert C. Waag, "Propagation and Backpropagation for Ultrasonic Wavefront Design," IEEE Trans. UFFC, vol. 44, no. 1, Jan. 1997

[13] Dan E. Dudgeon and Russell M. Mersereau, “Multidimensional Digital Signal Processing,” Prentice Hall, 1984. See especially Chapter 1.4, “Sampling Continuous 2-D Signals.”

[14] Monson H. Hayes, “The Reconstruction of a Multidimensional Sequence from the Phase or Magnitude of its Fourier Transform,” IEEE Trans. ASSP, vol. 30, no. 2, Apr. 1992

[15] Athanasios Papoulis, “Signal Analysis,” McGraw-Hill, 1977. See especially Chapter 5-1, “Sampling and Interpolation.”

[16] J. Nelson Wright et. al., “Method and Apparatus for Coherent Image Formation,” US Patent 5,623,928, Apr. 1997

[17] S. Freeman, Pai-Chi Li, and M. O’Donnell, “Retrospective Dynamic Transmit Focusing,” Ultrasonic Imaging, vol. 17, no. 3, Jul.1995

